Bioorganic Chemistry 147 (2024) 107392

Contents lists available at ScienceDirect

Bioorganic Chemistry

journal homepage: www.elsevier.com/locate/bioorg

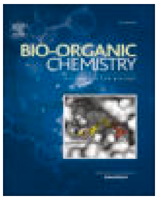

Synthesis of obovatol and related neolignan analogues as α-glucosidase and α-amylase inhibitors

Claudia Sciacca [a], Nunzio Cardullo [a], Luana Pulvirenti [b], Gabriele Travagliante [a], Alessandro D'Urso [a], Roberta D'Agata [a], Emanuela Peri [c], Patrizia Cancemi [c], Anaëlle Cornu [d], Denis Deffieux [d], Laurent Pouységu [d], Stéphane Quideau [d,e,*], Vera Muccilli [a,**]

[a] *Department of Chemical Sciences, University of Catania, V.le A. Doria 6, 95125 Catania, Italy*
[b] *CNR-ICB, Consiglio Nazionale delle Ricerche-Istituto di Chimica Biomolecolare, via Paolo Gaifami 18, Catania 95126, Italy*
[c] *Department of Biological Chemical and Pharmaceutical Sciences and Technologies, University of Palermo, Palermo 90128, Italy*
[d] *Univ. Bordeaux, ISM (CNRS-UMR 5255), 351 cours de la Libération, Talence Cedex, France*
[e] *Institut Universitaire de France, 1 rue Descartes, 75231 Paris Cedex 05, France*

ARTICLE INFO

Keywords:
Neolignans
Circular dichroism analysis
Intrinsic fluorescence quenching
Michael-type addition
Ullmann coupling
α-amylase inhibition
α-glucosidase inhibition
Surface plasmon resonance imaging
Cytotoxicity

ABSTRACT

Diabetes mellitus is a metabolic disease characterized by hyperglycemia, which can be counteracted by the inhibition of α-glucosidase (α-Glu) and α-amylase (α-Amy), enzymes responsible for the hydrolysis of carbohydrates. In recent decades, many natural compounds and their bioinspired analogues have been studied as α-Glu and α-Amy inhibitors. However, no studies have been devoted to the evaluation of α-Glu and α-Amy inhibition by the neolignan obovatol (**1**). In this work, we report the synthesis of **1** and a library of new analogues. The synthesis of these compounds was achieved by implementing methodologies based on: phenol allylation, Claisen/Cope rearrangements, methylation, Ullmann coupling, demethylation, phenol oxidation and Michael-type addition. Obovatol (**1**) and ten analogues were evaluated for their *in vitro* inhibitory activity towards α-Glu and α-Amy. Our investigation highlighted that the naturally occurring **1** and four neolignan analogues (**11**, **22**, **26** and **27**) were more effective inhibitors than the hypoglycemic drug acarbose (α-Amy: 34.6 μM; α-Glu: 248.3 μM) with IC$_{50}$ value of 6.2–23.6 μM toward α-Amy and 39.8–124.6 μM toward α-Glu. Docking investigations validated the inhibition outcomes, highlighting optimal compatibility between synthesized neolignans and both the enzymes. Concurrently circular dichroism spectroscopy detected the conformational changes in α-Glu induced by its interaction with the studied neolignans. Detailed studies through fluorescence measurements and kinetics of α-Glu and α-Amy inhibition also indicated that **1**, **11**, **22**, **26** and **27** have the greatest affinity for α-Glu and **1**, **11** and **27** for α-Amy. Surface plasmon resonance imaging (SPRI) measurements confirmed that among the compounds studied, the neolignan **27** has the greater affinity for both enzymes, thus corroborating the results obtained by kinetics and fluorescence quenching. Finally, *in vitro* cytotoxicity of the investigated compounds was tested on human colon cancer cell line (HCT-116). All these results demonstrate that these obovatol-based neolignan analogues constitute promising candidates in the pursuit of developing novel hypoglycemic drugs.

1. Introduction

Obovatol (**1**), magnolol (**2**) and honokiol (**3**) are phenylpropanoid neolignans isolated for the first time from the *Magnolia* genus (Fig. 1) [1,2]. These three compounds have been reported for several pharmacological relevant properties as antioxidant [3,4], antiproliferative [5,6], antibacterial [7,8], cytotoxic [6], neuro- and hepatoprotective [9,10], anti-inflammatory [11,12], anti-platelet [13], anxiolytic [1] antidepressant [14], and anti-obesity agents [15]. Several studies have been devoted to the synthesis of **2** [16] and **3** [17], as well as structural analogues thereof [18–23]. However, much less has been reported for **1** [24,25], which is extracted in low yields from *Magnolia obovata* dried

---

* Corresponding author at: Univ. Bordeaux, ISM (CNRS-UMR 5255), 351 cours de la Libération, Talence Cedex, France.
** Corresponding author at: Department of Chemical Sciences, University of Catania, V.le A. Doria 6, 95125 Catania, Italy.
E-mail addresses: stephane.quideau@u-bordeaux.fr (S. Quideau), v.muccilli@unict.it (V. Muccilli).

https://doi.org/10.1016/j.bioorg.2024.107392
Received 8 December 2023; Received in revised form 12 April 2024; Accepted 21 April 2024

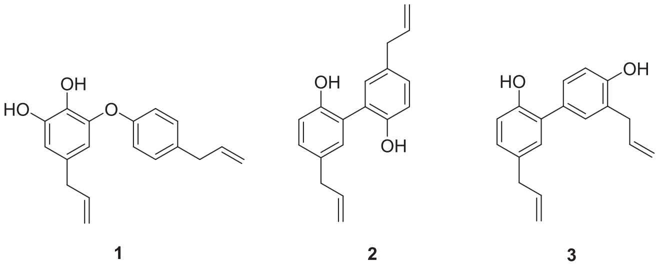

Fig. 1. Structures of obovatol (**1**), magnolol (**2**) and honokiol (**3**).

bark (0.26 %) and leaves (0.76 %). Therefore, the biological activities of **1** or its analogues are still poorly explored.

Magnolol (**2**) and honokiol (**3**) are also inhibitors of α-glucosidase and α-amylase [26–29]. The inhibition of these enzymes is one of the established approaches proposed to manage type 2 diabetes by delaying carbohydrate metabolism [30,31]. The approved antidiabetic drug acarbose is also a good α-glucosidase and α-amylase inhibitor [32,33], but undesired side effects including flatulence, diarrhea, abdominal distention and nausea, have been reported [33,34]. This is the reason why a search of novel inhibitors of these enzymes has been initiated and natural product-based compounds such as the biaryl magnolol and some of its derivatives were notably found to be promising alternatives for inhibiting α-glucosidase. The inhibitory activity of magnolol itself (**2**) was not as strong as some of its derivatives, but still was by far much higher than that of the pseudotetrasaccharide acarbose and that of its biaryl isomer honokiol (**3**) [26]. These results led us to contemplate the case of obovatol (**1**), a catecholic diaryl ether analogue of **2** and **3**.

We started this study by carrying out the chemical synthesis of **1**, for which the diaryl ether linkage was forged by an Ullman coupling reaction [35]. A small library of novel obovatol-inspired compounds, including derivatives exhibiting various functional groups (methoxy, bromide, carboxyl and formyl groups) and diaryl thioether analogues, was also synthesized in the aim of gathering structure–activity data related to the inhibition of α-glucosidase and α-amylase in the light of previous findings [36–39]. All of these compounds were subjected to *in vitro* biochemical assays, kinetic analysis, fluorescence, circular dichroism spectroscopies, surface plasmon resonance imaging (SPRI), and *in silico* modeling. In addition, *in vitro* cytotoxicity of the examined compounds was tested toward HCT-116, a human colorectal carcinoma cell line of Duke's type A, with an epithelial morphology, initiated from a 48-year-old male.

2. Results and discussion

2.1. Chemistry

The synthesis of obovatol (**1**) was designed according to the approach depicted in Scheme 1. The ultimate dimethylated intermediate **9** could be prepared through a copper-mediated Ullmann coupling reaction between the aryl bromide **7** and the commercial 4-allylphenol (**8**). The aryl bromide **7** could be obtained from the commercial 3-bromocatechol (**4**) through a regioselective monoallylation, a Claisen/Cope cascade rearrangement and a final methylation reaction.

Thus, we proceeded accordingly to synthesize **1** in five steps, starting with the preparation of 2-allyloxy-3-bromophenol **5** from **4** using allyl bromide (Scheme 2). The *O*-allylated compound **5** was then subjected to a Lewis acid-mediated [3,3] sigmatropic Claisen rearrangement, which was followed in situ by a [3,3] sigmatropic Cope rearrangement [40] to deliver the intermediate **6** in 80 % yield. This catechol was next methylated under mild conditions to give the desired aryl bromide **7** in 70 % yield (Scheme 2).

The copper-catalyzed Ullmann coupling reaction, which is one the most useful methods for the formation of diaryl ethers [41], was then performed between **7** and **8** using *N*,*N*-dimethylglycine hydrochloride (30 mol%) as a ligand allowing the use of catalytic amount of the copper (I) iodide catalyst (10 mol%) [35,42] in the presence of Cs_2CO_3 as a base in dioxane at 90 °C. The resulting coupling product **9** was obtained in 52 % yield and was demethylated in 84 % yield using boron tribromide (BBr_3). This total synthesis of obovatol (**1**) was thus achieved in a satisfying overall yield of 15 % (Scheme 2). Slight modifications of the BBr_3-mediated demethylation conditions enabled us to produce two additional compounds, the mono-demethylated variant **10** and the bis-hydrobrominated derivative **11** (Scheme 3), which were respectively obtained in overall yields of 18 % and 10 % from 3-bromocatechol (**4**).

The Ullmann coupling-based strategy used for the synthesis of **1** turned out to be a practical approach to a variety of diaryl ether obovatol analogues. As depicted in Scheme 4, eugenol (**12**) could be coupled with 1-allyl-4-bromobenzene (**13**), 2-bromo-4-methoxyphenyl acetic acid (**16**) and 4-bromobenzoylchloride (**18**) to respectively afford compounds **14** (94 % yield), **17** (40 % yield) and **19** (20 % yield). The demethylation of **14** gave the analogue **15** (97 % yield). Additionally, 4-allylphenol (**8**) reacted with 5-bromo-2-methoxybenzaldehyde (**21**) to give **22**.

The preparation of diaryl thioether analogues could not be achieved by Ullmann coupling reactions, so we relied on an alternative route involving the intermediacy of an electrophilic *ortho*-quinone species derived from the oxygenative demethylation of a 2-methoxyphenol.

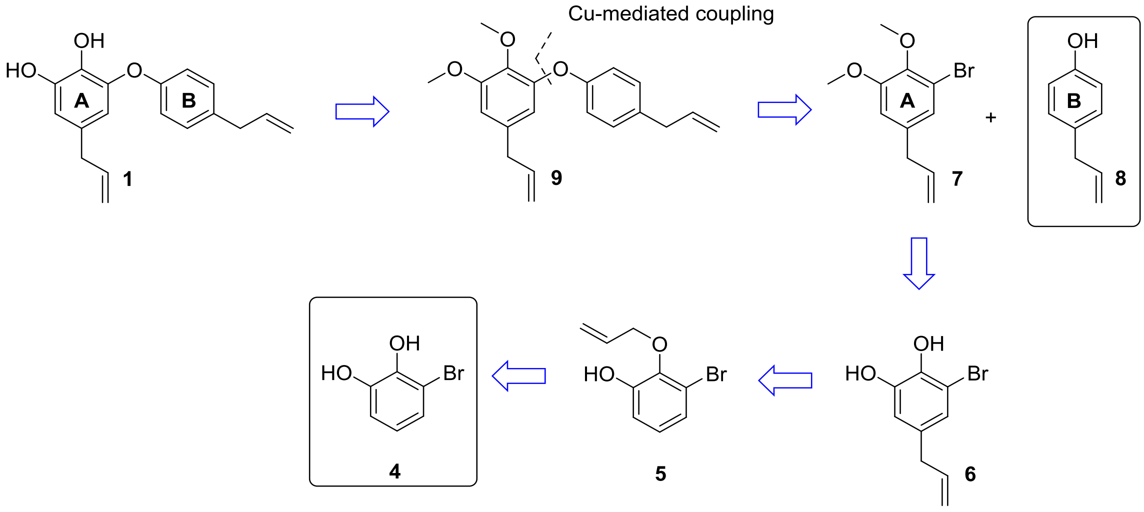

Scheme 1. Retrosynthetic analysis of obovatol (**1**).

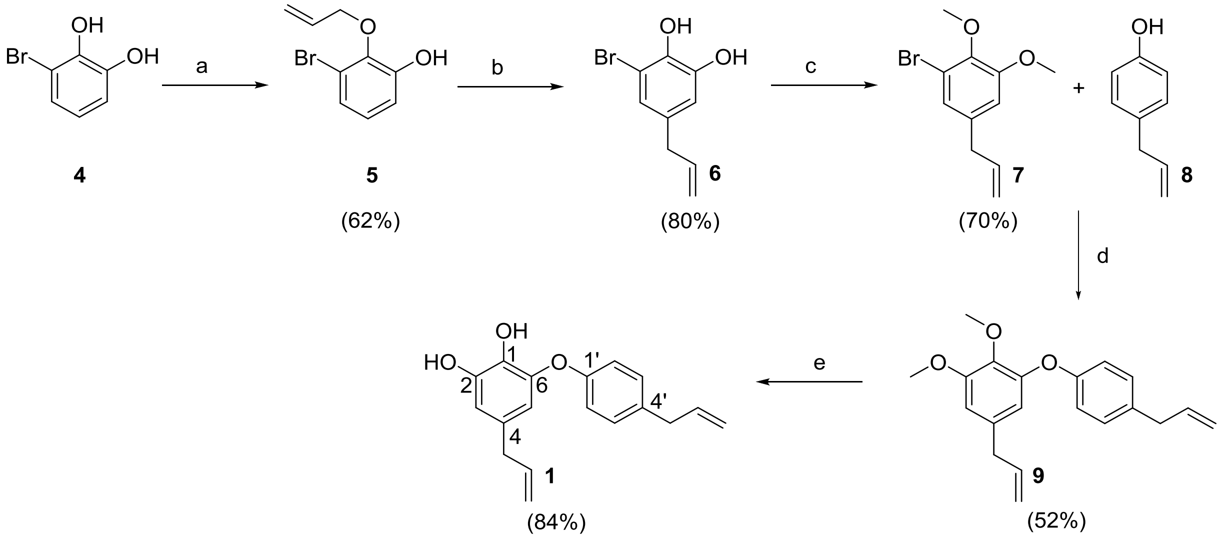

Scheme 2. Syntheis of obovatol (**1**). *a)* dry acetone, K_2CO_3 (1 eq.), allyl bromide (1.4 eq.), 6 h, 56 °C. *b)* dry CH_2Cl_2, 1 M Et_2AlCl (in dry *n*-hexane, 2 eq.), 3 h, room temperature. *c)* DMF, K_2CO_3 (2 eq.), CH_3I (3 eq.), 4 h, room temperature. *d)* dioxane, Cs_2CO_3 (2 eq.), 4-allylphenol (**8**, 1.5 eq.), CuI (10 mol%), *N*, *N*-dimethylglycine HCl (30 mol%), 52 h, 90 °C. *e)* BBr_3 (1 M in CH_2Cl_2, 2 eq.), dry CH_2Cl_2, 3 h, –78 °C.

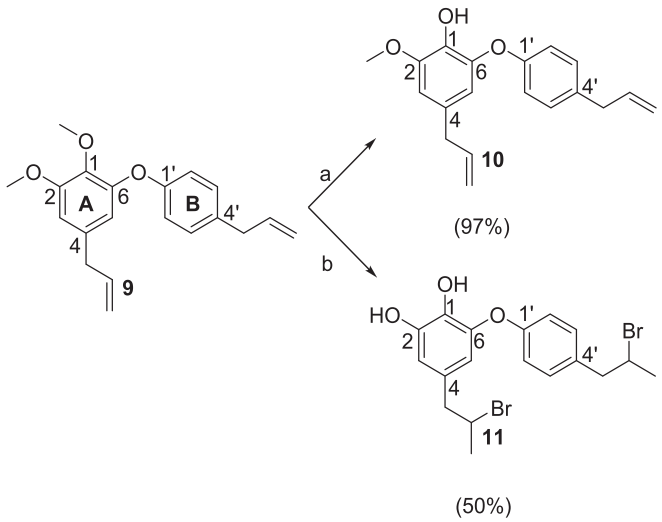

Scheme 3. Synthesis of analogues **10**–**11**. *a)* BBr_3 (1 M in CH_2Cl_2, 1 eq.), dry CH_2Cl_2, 2 h, –78 °C. *b)* BBr_3 (1 M in CH_2Cl_2, 1 eq.), dry CH_2Cl_2, 30 min, –78 °C, then room temperature, 2 h.

Thus, eugenol (**12**) was oxygenatively demethylated with the "stabilized" nonexplosive formulation of 2-iodoxybenzoic acid (SIBX) to generate the intermediate **23** [43,44]. This *ortho*-quinone was then directly treated in situ with either thiophenol (**24**) or 4-bromothiophenol (**25**), which reacted in a regioselective 1,6-conjugate manner with **23** to afford compounds **26** and **27** in 45 and 35 % yields, respectively, from eugenol (**12**) (Scheme 5).

2.2. *In vitro α-glucosidase and α-amylase inhibitory activity*

Obovatol (**1**) and its synthetized analogues were evaluated for their *in vitro* inhibitory activity towards α-glucosidase from *Saccharomyces cerevisiae* (α-Glu) and α-amylase from porcine pancreas (α-Amy) according to the previously described spectrophotometric methods [45]. The antidiabetic drug acarbose was employed as a positive control in both assays. The inhibitory activity was expressed as the concentration (μM) inhibiting 50 % of the enzyme activity (IC_{50}); thus, the lower the IC_{50} value, the higher the inhibitor activity. The data obtained for both enzymes are reported in Table 1.

According to the results, obovatol (**1**) is twice as active as α-Glu inhibitor (124.6 μM) and a slightly better α-Amy inhibitor (23.6 μM) than acarbose (248.3 μM and 34.6 μM, respectively). Moreover, most of the analogues are more active than **1** toward the inhibition of α-Glu (39.8 – 97.7 μM) and by far more potent than acarbose. These neolignan derivatives have α-Amy inhibitory activity with IC_{50} value in the range of 6.2 – 43.6 μM. Among these, **11**, **19**, and **27** (6.2 – 17.6 μM) are more active than both **1** (23.6 μM) and acarbose (34.6 μM). All compounds are more effective inhibitors of α-Amy than of α-Glu, and can thus be considered as potential drug alternatives to acarbose.

Some speculations about the structure–activity relationship can be made by considering the different structural modifications brought to the native obovatol structure. Compounds with free hydroxyl groups exhibit a significant inhibitory effect in agreement with previous findings [46,47]. Thus, methylated compounds **9** and **10** were less active than the catecholic **1**, and methylated **14** was less active than the parent compound **15**. Moreover, the brominated catecholic compound **11** shows an IC_{50} value of 12.7 μM for α-Amy inhibition and 111.0 μM for α-Glu inhibition. The higher inhibition activity of **11** with respect to that of obovatol (**1**) might be attributed to the presence of 2-bromopropyl chains instead of the allyl ones. The combined effect of the free hydroxyl groups and the presence of bromine atoms contributes to the overall inhibitory activity not only of the neolignan derivative **11**, but also of the thioether analogue **27** (6.2 μM for α-Amy inhibition and 39.8 μM for α-Glu inhibition). The other diaryl thioether compound **26** is also among the most active compounds tested against α-Glu (56.1 μM). This higher activity observed with the sulfide analogues has been previously documented in other thioether compounds for α-glucosidase [38], but not for α-amylase. The role of bromine atoms on aromatic and aliphatic moieties (β-carboline derivatives, benzimidazole-thioquinolines, arylketones) in increasing α-Glu inhibitory activity has already been studied [36,48,49]. According to the data reported in Table 1, bromine atoms may also be important in enhancing the α-Amy inhibition. Compounds **11** and **27** are the most active compounds tested against α-Amy, showing respectively IC_{50} value of 6.2 and 17.6 μM.

Compound **15** differs from obovatol (**1**) by the position of the allyl chain onto the ring A and the absence of an OH group at C-2. Nevertheless, **15** has the same activity as its natural lead, and this result may suggest that the allyl chain position is not important for the interaction with both enzymes. Finally, compounds **17**, **19**, and **22**, maintaining only the 1-allyl-4-phenoxy moiety of obovatol (ring B, Fig. 2), but

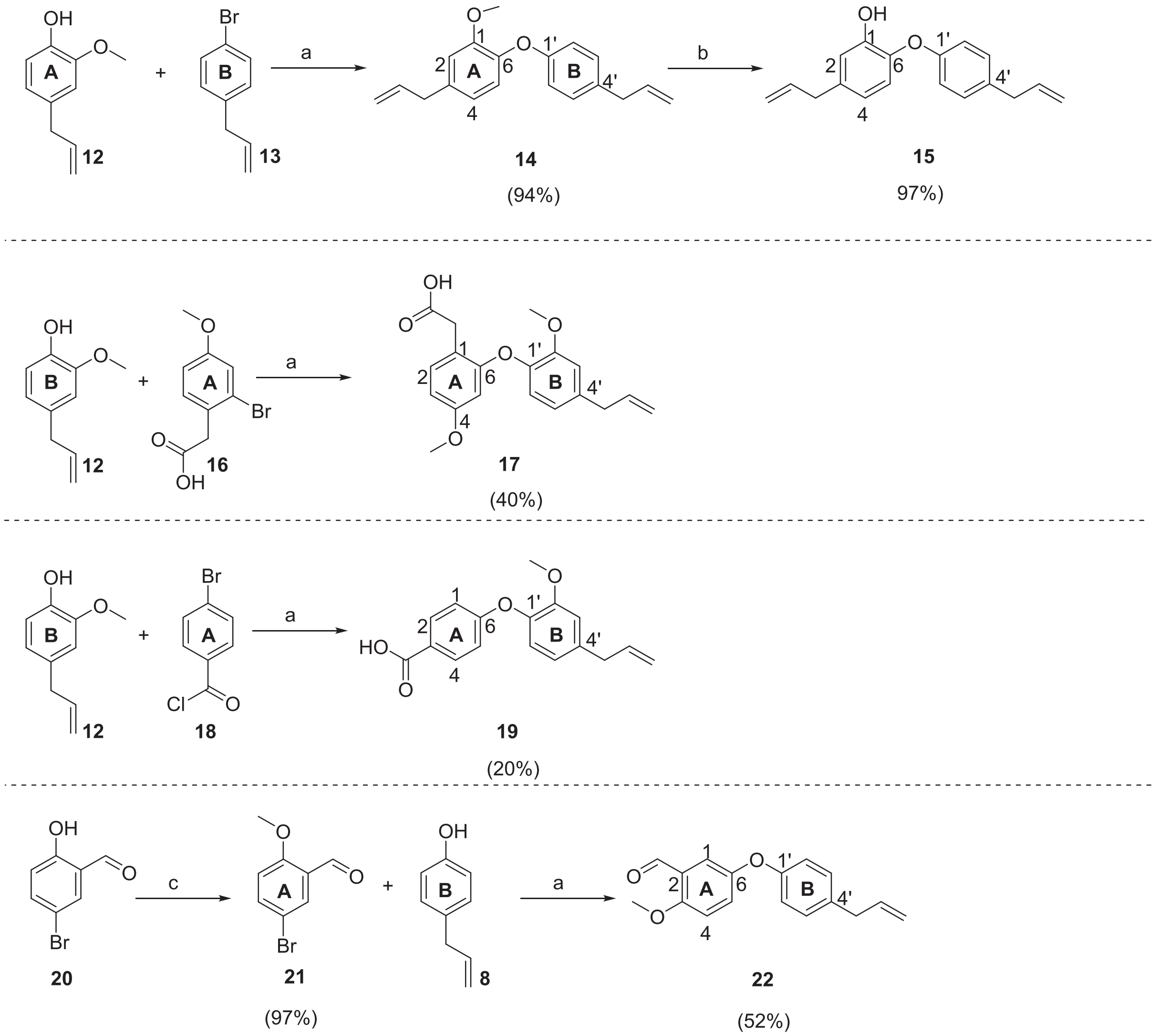

Scheme 4. Synthesis of analogues **14**, **15**, **17**, **19** and **22**. *a)* dioxane, Cs_2CO_3 (2 eq.), phenol (1.5 eq.), CuI (10 mol%), *N*,*N*-dimethylglycine HCl (30 mol%), 24 h, 90 °C. *b)* BBr_3 (1 M in CH_2Cl_2, 1 eq.), dry CH_2Cl_2, 3 h, –78 °C. *c)* DMF, K_2CO_3 (3 eq.), CH_3I (3 eq.), overnight, room temperature.

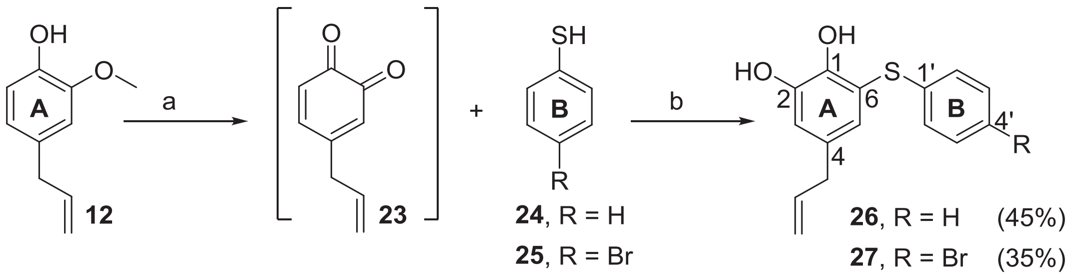

Scheme 5. Synthesis of thioether analogues **26** and **27**. *a)* SIBX (2.15 eq.), dry THF, 16 h, room temperature. *b)* thiol (3 eq.), dry THF, 1–2 h, room temperature.

lacking any allyl chain on the ring A, are as active as **1** and even more effective as α-Glu inhibitor. These data suggest that the presence of an allyl chain on these diaryl ether structures may not be relevant for the activity. More in detail, compounds **17** and **19**, bearing a carboxyl function onto the ring A instead of an allyl chain have comparable or slightly better inhibitory activities than obovatol toward both enzymes. It is worth noting that compound **22**, bearing a formyl group onto the ring A, is a more effective α-Glu inhibitor than obovatol. The structure–activity relationships described above are graphically summarized in Fig. 2.

2.3. Molecular modelling

To rationalize the *in vitro* inhibitory outcomes, the obovatol analogues were evaluated *in silico* for their affinity to the α-glucosidase and α-amylase catalytic sites and the output poses were carefully analyzed (Fig. 3 and 4). The 3D structure of α-Glu from *S. cerevisiae* (AF-P53341-F1-model_v4) was downloaded from AlphaFold data bank, and that of α-Amy (PDB ID: 4 W93) from the Protein Data Bank. Glide Ligand Docking was employed to perform the computational experiments (see the Experimental Section for more details). The *in silico* data for α-Glu

Table 1

Inhibitory activity (IC_{50}) towards α-Amy and α-Glu.

Compounds	α-Amy[a] IC_{50} ± SEM	α-Glu[a] IC_{50} ± SEM
1	23.6 ± 2.0 ***	124.6 ± 3.0 ***
9	43.6 ± 3.5 ***	198.0 ± 15.6 ***
10	38.8 ± 2.9	167.5 ± 5.6 ***
11	12.7 ± 0.9 ***	111.0 ± 7.3 ***
14	36.1 ± 2.8	177.7 ± 2.9 ***
15	24.5 ± 2.1 ***	127.7 ± 5.8 ***
17	20.1 ± 0.4 ***	97.7 ± 2.0 ***
19	17.6 ± 1.6 ***	119.4 ± 4.5 ***
22	27.0 ± 2.3 *	65.6 ± 2.1 ***
26	35.4 ± 1.2	56.1 ± 2.4 ***
27	6.2 ± 1.0 ***	39.8 ± 2.4 ***
Acarbose	34.6 ± 0.9	248.3 ± 2.3

*P < 0.05, ***: P < 0.001, compared with the group of acarbose.

[a] Results are expressed in μM. IC_{50} is the concentration required to inhibit 50 % of enzyme activity.

and α-Amy are listed in Tables 2 and 3; these values suggest a good interaction of the obovatol analogues with both proteins. In general, by carefully analyzing the pose outcomes, it is possible to observe that all the ligands are compatible with the hydrophobic pocket of both enzymes, suggesting that they could be promising inhibitory agents. The docking analysis of obovatol (**1**) shows a stabilization into the hydrophobic pocket of the catalytic site of α-Glu due to the formation of a hydrogen bond between the OH group at C-2 and Asp408, a π-cation interaction between the A-ring and Arg312, and a π-π interaction between the B-ring and Phe300 (Fig. 3). Moreover, upon visual examination, it seems that the allyl chain on the B-ring of **1** is stabilized by the hydrophobic portion (Ala278, Val277, Ala21, Gly217, and Leu218) within the catalytic site (IC_{50}: 124.6 μM). When the OH group at C-2 is methylated, as in compound **10** (Scheme 3), the ligand changes its orientation into the binding pocket, thus favoring the formation of a hydrogen bond between the OH group at C-1 and Glu304, but maintaining the π-cation interaction with Arg312 (docking affinity: –3.35 Kcal/mol, IC_{50}: 167.5 μM; see Fig. S8). In the case of **9** in which both OH groups at C-1 and C-2 are methylated, the ligand is capable of forming two π-π interactions between the B- and A-rings and the α-Glu Phe177 and Phe300 residues (docking affinity: –5.52 Kcal/mol, IC_{50}: 198.0 μM) and a π-π interaction between A-ring and the α-Amy Trp59 (docking affinity: –4.64 Kcal/mol, IC_{50}: 43.6 μM; Table 3). However, despite these interactions, the methylation of OH groups at the C-1 and C-2 positions does not represent an advantageous structural modification due to the absence of H-donor interactions.

If methylation of the phenolic OH groups thus did not seem beneficial for the biological activity, the hydrobromination of both allyl chains would appear to be. Indeed, ligand **11** shows better binding energies for both enzymes (–5.04 and –4.83 Kcal/mol). These data obtained for α-Glu and α-Amy are also confirmed by the IC_{50} values (111 μM and 12.7 μM, see Section 2.2). Taking a look to the docking pose of **11** into α-Glu, it seems that the flexibility of the aliphatic chains associated with the hydrophobic effect of the bromine atom(s) surrounded by a hydrophobic portion (Phe177, Leu218, Ala278, Phe300, Phe158, Phe157, Pro309, Phe310, Phe311) allows the ligand incorporation into the cavity, reducing the exposure to the external environment. This favors the formation of two hydrogen bonds between the OH groups at C-1 and C-2 and Asp349, while the B-ring establishes a π-cation interaction with Arg312. Similar considerations are related to the docking into α-Amy. The ligand **11** seems to be incorporated into the α-Amy binding site in a way that the A-ring changes its orientation, favoring the formation of two hydrogen bonds between the OH group at C-1 with His299, and the OH group at C-2 with Glu233.

Ligands **14** and **15** maintain the B-ring of obovatol (**1**), whereas the substitution on the A-ring differs from **1** with the allylic chain at C-3 and a methoxy (**14**) or a hydroxy group (**15**) at C-1. The outcomes obtained for both enzymes highlight the fact that the lack of a OH group at the C-2 position worsens the stability of the complex (α-Glu: ΔG_{bind} –2.84 and IC_{50}: 127.7 μM (**15**); ΔG_{bind} –3.02 Kcal/mol and IC_{50}: 177.7 μM (**14**); α-Amy: ΔG_{bind} –3.30 and IC_{50}: 24.5 μM (**15**); ΔG_{bind} –2.70 Kcal/mol and IC_{50}: 36.1 μM (**14**)). The structural modifications on the A-ring of ligands **17** (carboxymethyl group at C-1) and **19** (carboxyl group at C-3) seem to have no significant effect on the stabilization of the corresponding complexes with α-Glu, and consequently, they have comparable inhibitory activity to that of **1**. However, for α-Amy, both ligands are well accommodated within the hydrophobic pocket with a ΔG_{bind} of –5.09 (IC_{50}: 97.7 μM); and –5.02 Kcal/mol (IC_{50}: 119.4 μM), respectively, suggesting a certain stability of the complexes with the biological target. Compound **17** can establish a hydrogen bond between the carbonyl oxygen of the carboxymethyl group and Gln63. Moreover, the A-ring establishes two π-π stacking interactions with Trp58 and Trp59. Ligand **19** has a different orientation into the hydrophobic pocket as compared to that of **17**, establishing two accepting hydrogen bonds between the two oxygens of the carboxyl group in the C-3 position and the Lys200 and Ile235 residues. Moreover, the A-ring is also involved in a π-π interaction with His201. In both ligands, the B-ring does not participate in the interaction with α-Amy and appears to be more exposed to the external environment. Finally, the formyl group on the A-ring of ligand **22** is involved in the formation of a hydrogen bond with His239 of the α-Glu hydrophobic pocket, contributing to the good stabilization energy of –4.66 Kcal/mol (IC_{50}: 65.6 μM) that was observed. Analogously, a hydrogen bond between the carbonyl group and Ile235 and a π-π stacking interaction between the A-ring and His201 occur within the α-Amy catalytic site. In both cases, no stabilization effect was due to the B-ring as observed for **1**.

The most active compounds toward the inhibition of α-Glu are the diaryl thioethers **26** and **27,** according to the *in vitro* assay results. Docking analyses corroborated these results as indicated by calculated ΔG_{bind} (**26**: docking affinity –5.34 Kcal/mol and IC_{50}: 56.1 μM; **27**: docking affinity –5.37 Kcal/mol and IC_{50}: 39.8 μM). The ligand **26** interacts with the catalytic pocket only through the A-ring, establishing a hydrogen bond between the OH group at C-2 and Asp349, whereas the

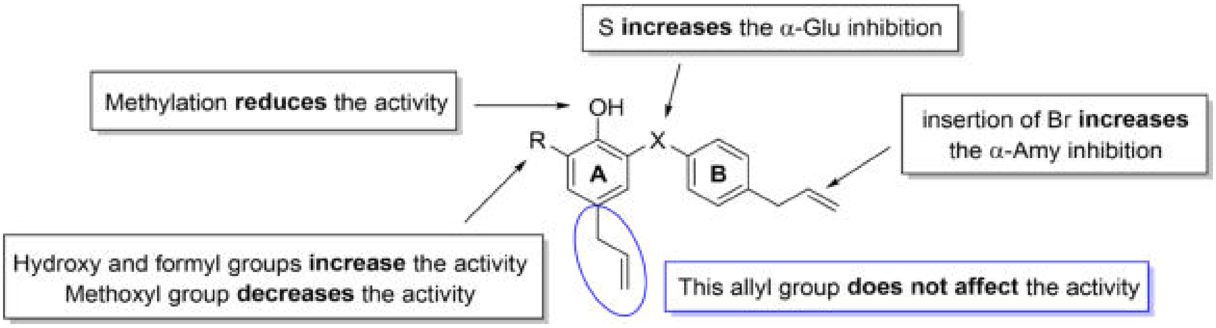

Fig. 2. Structural features affecting the α-Amy and α-Glu inhibitory activity of obovatol analogues.

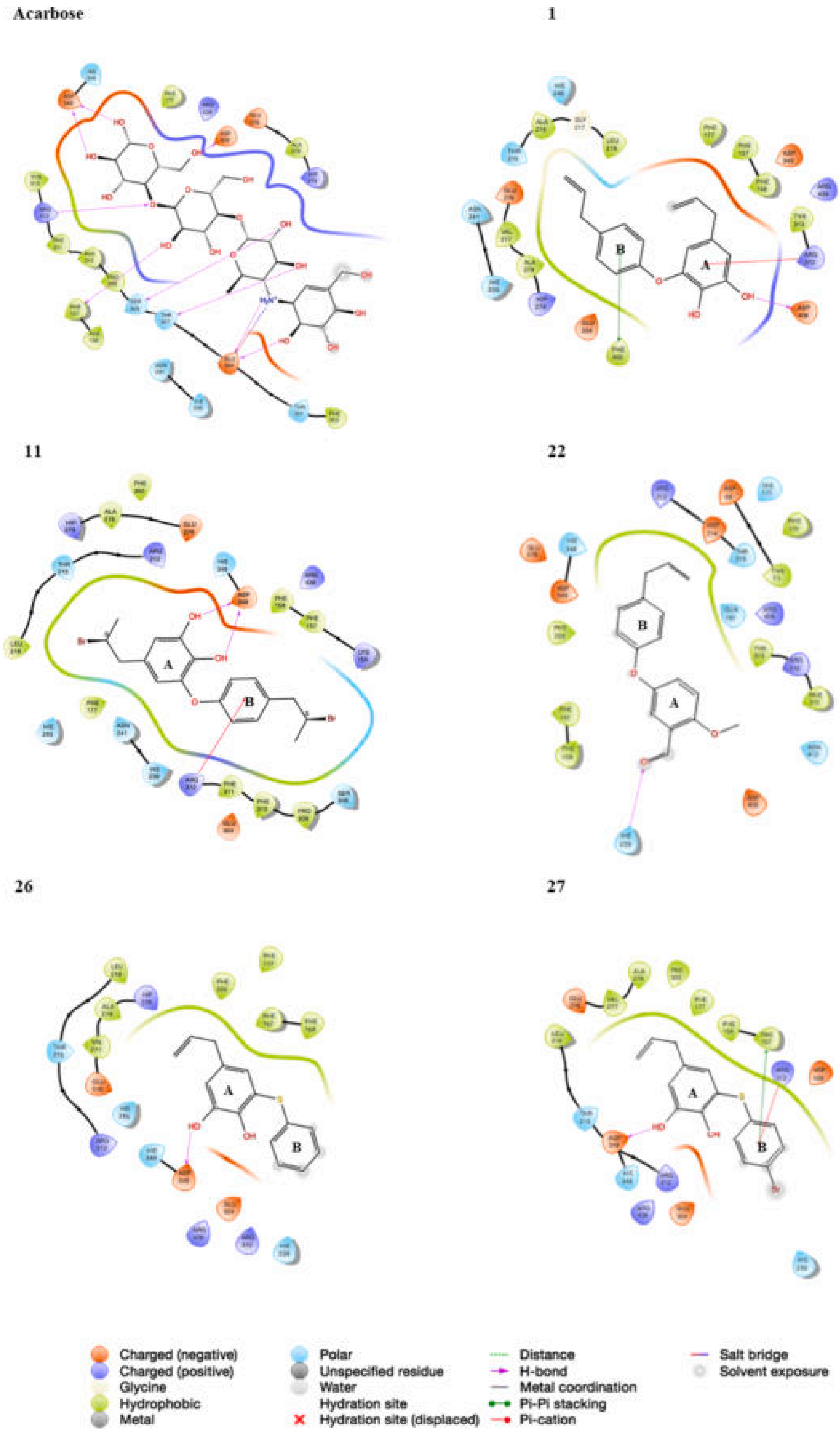

Fig. 3. 2D interaction diagrams of **acarbose**, **1**, **11**, **22**, **26** and **27** with α-glucosidase.

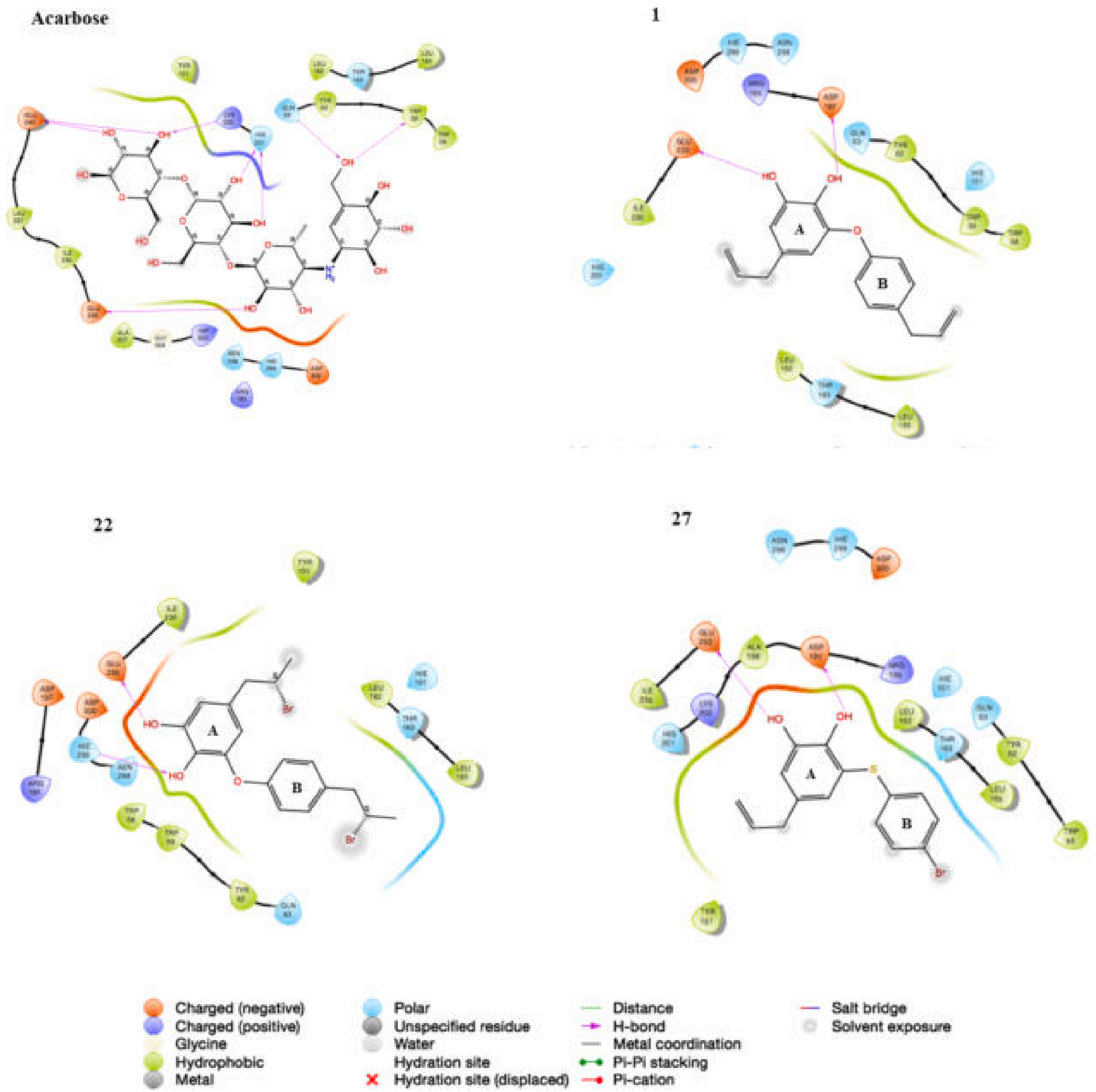

Fig. 4. 2D interaction diagrams of **acarbose**, **1**, **11**, and **27** with α-amylase.

B-ring does not have a role in the stabilization of the complex, being more exposed to the external environment. However, the introduction of a bromine substituent on the B-ring, as in ligand **27**, allows the formation of a π-cation and a π-π interaction with the close Arg312 and Phe157 residues, thus justifying the higher inhibitory activity with respect to **26**. It seems that the combined presence of the thioether link and the bromine atom makes the interaction with the enzyme more stable and, consequently, the inhibition effect obtained is higher than that of obovatol (**1**). The ligand **27** is also efficient in stabilizing the complex with α-Amy (docking affinity –5.50 Kcal/mol and IC_{50}: 6.2 μM). The A-ring mimics the obovatol maintaining the same interactions, but being more incorporated and less exposed to the external environment. The B-ring is better accommodated and surrounded by a hydrophobic portion (Tyr151, Ile215, Ala198, Leu162, Leu165, Tyr62, Trp59) of α-Amy that contributes to stabilize altogether the complex (Fig. 4). These observations perfectly agree with its IC_{50} value and allow us to consider **27** as a potent α-Amy inhibitor.

Therefore, considering the above data, the most important outcome is that OH groups at C-1 and mostly at C-2 of the obovatol scaffold are relevant for the interaction with α-Glu and α-Amy. In particular, the OH group in position C-1 would seem to have a key role in the stabilization of the complex, since when it is involved in the formation of hydrogen bonds with any of the two proteins, the complex is more stable and consequently the inhibitory effect is stronger. Compounds **11**, **26**, and **27** are among the most active ligands for α-Glu. A hydrogen bond forms between the OH group at C-2 and Asp349, a component of the catalytic triad of α-Glu (consisting of Asp214, Glu276, and Asp349). This interaction appears crucial for stabilizing the transition state derived from the native substrate, as indicated by a previous study [50]. Analogously, into α-Amy cavity, ligands **11** and **27** establish a hydrogen bond between the OH group at C-2 and Glu233, which is also part of the catalytic triad [50]. In this context, when this substitution pattern on A-ring is retained, the B-ring seems to have only a supporting role.

Additionally, the absorption, distribution, metabolism, and excretion (ADME) profile of obovatol (**1**), **11**, **22**, **26**, and **27** was determined using the SwissADME web platform [51]. The results are reported in Figs. S3 – S7. All compounds show a computational TPSA (topological polar surface area) less than 140 Angstroms squared [$Å^2$]), between

Table 2
Binding Energies (ΔG_{bind}) and list of molecular interactions and residues interacting with obovatol and its analogues within the α-Glu catalytic site.

Ligands	Glide calcd ΔG_{bind}	Interacting residues	Interaction	Distance (A°)
acarbose				
	–7.09	Glu304, Thr307, Ser308, Arg312, Phe157, Asp408, Asp349		
1				
B-ring	–3.69	Phe300	π – π	–
A-ring		Arg312	π-cation	–
OH (C-2)		Asp408	H-donor	2.1
9				
B-ring	–5.52	Phe177	π – π	–
A-ring		Phe300	π – π	–
10				
OH (C-1)	–3.35	Glu304	H-donor	1.9
A-ring		Arg312	π-cation	–
11				
OH (C-1)	–5.04	Asp349	H-donor	1.7
OH (C-2)		Asp349	H-donor	1.9
B-ring		Arg312	π-cation	–
14				
B-ring	–3.02	Phe300	π – π	–
B-ring		Phe157	π – π	–
15				
OH (C-1)	–2.84	Glu304	H-donor	1.8
A-ring		Phe157	π – π	–
A-ring		Arg312	π-cation	–
17				
OCH_3 (C-4)	–4.61	Asn241	H-acceptor	2.0
COO^- (C-1)		Lys155	salt bridge	–
COO^- (C-1)		Arg312	H-acceptor	1.9
B-ring		Arg312	π-cation	–
19				
COO^- (C-3)	–4.14	Lys155	salt bridge	–
COO^- (C-3)		Arg312	H-acceptor	2.1
22				
CHO (C-2)	–4.66	Hie239	H-acceptor	2.1
26				
OH (C-1)	–5.34	Asp349	H-donor	1.9
OH (C-2)		Asp349	H-donor	1.6
27				
OH (C-1)	–5.37	Asp349	H-donor	1.9
OH (C-2)		Asp349	H-donor	1.6
B-ring		Phe157	π – π	–
B-ring		Arg312	π-cation	–

35.53 and 65.76 Å^2, thus computationally exhibiting good intestinal absorption [51]. Compounds **1**, **22**, and **26** show moderate solubility and a lipophilicity value (MlogP) less than 4.15, satisfying all Lipinsky's rules. Conversely, compounds **11** and **27** show a lipophilicity higher than 4.15, thus violating one Lipinsky's rule.

2.4. Kinetics of α-glucosidase and α-amylase inhibition

The mode of inhibition of the most active compounds in the inhibition of α-glucosidase (**1**, **11**, **22**, **26**, **27**) and/or α-amylase (**1**, **11**, **27**) was investigated by UV spectroscopy. Kinetics data were elaborated, plotting the reciprocal of initial velocity (ν_0) for each inhibitor concentration versus the reciprocal of substrate concentration [*p*-nitrophenyl-α-glucoside (NPG) for α-Glu and 2-chloro-4-nitrophenyl-α-maltotrioside (CNPG3) for α-Amy]. The results are reported as Lineweaver-Burk plots (L-B) in Fig. 5. The kinetic parameters are collected in Table 4. Secondary plots (Figures S11-S12) allowed the estimation of kinetic constants. The results were compared to previously published data on acarbose, reported as competitive inhibitor toward the two enzymes with K_i values of 3.7 and 6.9 μM, respectively [52–54]. Obovatol (**1**) and the most active synthetic compounds showed different mode of inhibition. Obovatol (**1**) resulted as a non-competitive inhibitor toward α-Glu as the lines in L-B plot cross the x-axis. A K_i value of 79.1 ± 2.1 μM (docking affinity: −3.69 Kcal/mol; IC_{50}: 124.6 μM) was determined for the formation of the enzyme-inhibitor (EI) complex by secondary plot, where the slope of each line of L-B plot (K_m/ν_{max}) was fitted

Table 3
Binding Energies (ΔG_{bind}) and list of molecular interactions and and residues interacting with obovatol and its analogues within the α-Amy catalytic site.

Ligands	Glide calcd ΔG_{bind}	Interacting residues	Interaction	Distance (A°)
acarbose				
	–8.33	Glu240, Glu233, Trp59, GLN63, His201, Lys200		
1				
OH (C-2)	–4.48	Glu233	H-donor	1.6
OH (C-1)		Asp197	H-donor	1.7
9				
A-ring	–4.64	Trp59	π – π	–
10				
OCH_3 (C-2)	–3.22	Gln63	H-acceptor	2.4
OH (C-1)		Tyr62	H-donor	2.7
11				
OH (C-2)	–4.83	Glu233	H-donor	1.6
OH (C-1)		Hie299	H-acceptor	2.7
14				
A-ring	–2.70	Trp59	π – π	–
15				
OH (C-1)	–3.30	Asp197	H-donor	1.8
17				
A-ring	–5.09	Trp58	π – π	–
A-ring		Trp59	π – π	–
COO^- (C-1)		Gln63	H-acceptor	2.0
19				
A-ring	–5.02	His201	π – π	–
COO^- (C-3)		Lys200	H-acceptor	2.5
COO^- (C-3)		Ile235	H-acceptor	1.9
22				
CHO (C-2)	–5.60	Ile235	H-acceptor	2.1
A-ring		His201	π – π	–
26				
B-ring	–4.99	His201	π – π	–
OH (C-1)		Glu233	H-donor	1.8
OH (C-2)		Glu233	H-donor	1.8
27				
OH (C-2)	–5.50	Glu233	H-donor	1.6
OH (C-1)		Asp197	H-donor	1.9

with obovatol concentration. The same inhibitory behaviour was observed for the analogues **11** (docking affinity: −5.04 Kcal/mol; IC_{50}: 111.0 μM and K_i values of 146.2 ± 5.8 μM) and **26** (docking affinity: −4.66 Kcal/mol; IC_{50}: 56.1 μM and K_i values of and 125.0 ± 5.1 μM). Differently, the data lines on the L-B plot of **22** and **27** suggested that these compounds act as mixed-type inhibitors, an intermediate mechanism between non-competitive and uncompetitive inhibition [46], as the lines intersected in the third quadrant (Fig. 5C and E). In this case, the inhibitor may bind to the enzyme into an allosteric site whether or not the enzyme has already bound the substrate. In this case, it is possible to determine the K_i value for the EI complex replotting the K_m/ν_{max} of L-B plot lines versus inhibitor concentration as described above. The K'_i related to the formation of the enzyme-substrate-inhibitor (ESI) complex, is obtained by replotting the intercept of L-B lines versus inhibitor concentration. For both inhibitors, K'_i values are lower than K_i, suggesting that these compounds could preferentially bind to the ES complex by interacting in a pocket different from the catalytic site. Worth noting, compound **27** showed a K_i value of 42.0 ± 2.3 μM and a K'_i 4.9 ± 0.2 μM, which are in agreement with the lowest IC_{50} (39.8 μM) value observed in the inhibitory assay and docking affinity −5.37 Kcal/mol. A lower K'_i than K_i in a mixed type inhibition is indicative of a preferential interaction of the inhibitor (in this case, **22** and **27**) in an allosteric site different from that occupied by the substrate. To support an α-glucosidase mixed-type inhibition of **22** and **27**, docking analysis on several potential allosteric sites was performed according to a literature report [55]. For each binding site, identified by SiteMap, the molecular interaction with both molecules was studied and the calculated ΔG_{bind} energies are reported in the Table S1 (see supporting). The best interaction was collected in the allosteric site with a sitescore of 1.001 and x,y,z coordinates of −8.56, 19.56, −6.89 (see Section 4.6 and Table S1), for which the calculated ΔG_{bind} was −5.97 and −6.21 kcal/mol for **22** and **27**, respectively. It is worth to note that these ΔG binding energies are lower with respect to those calculated for the same molecules into the catalytic site, suggesting a greater affinity with the

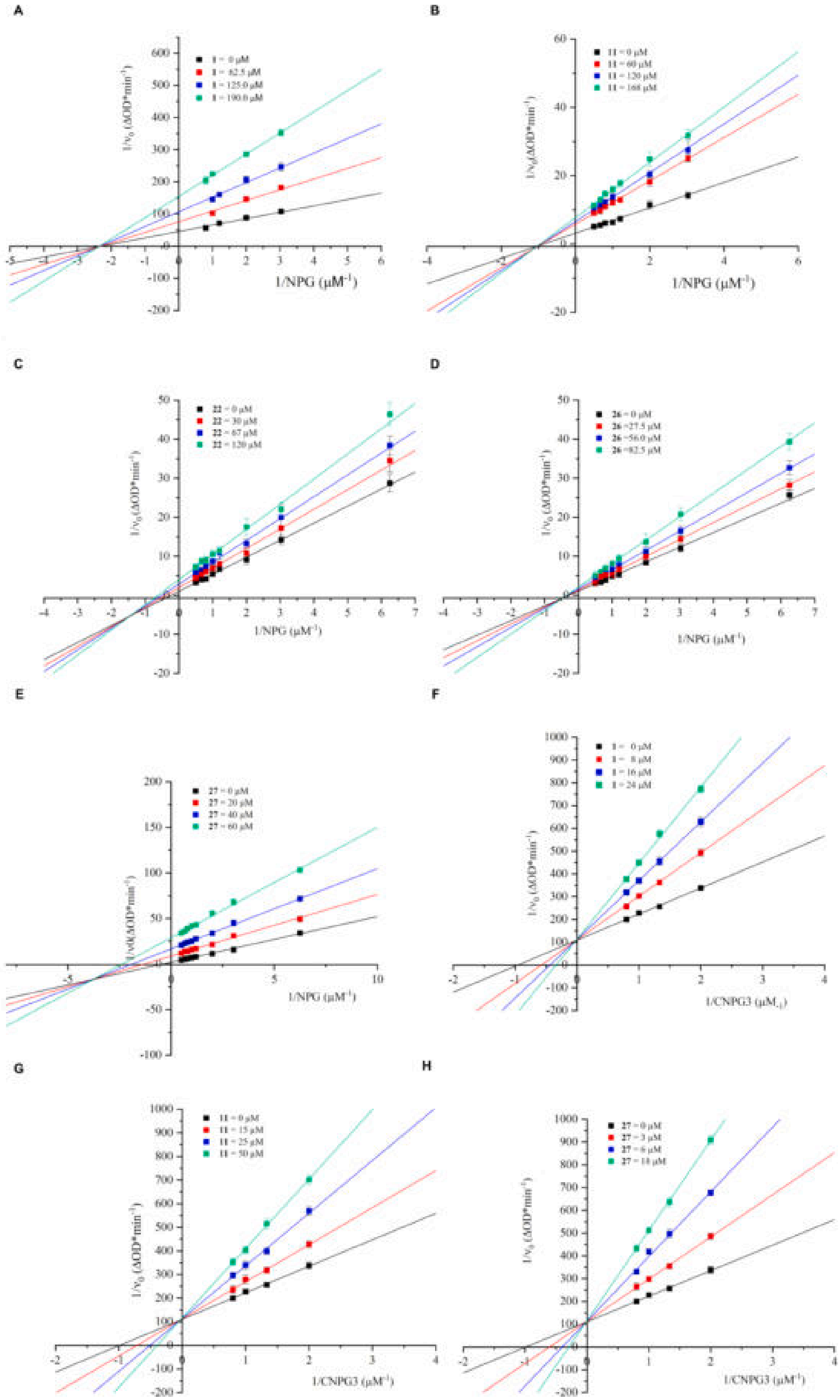

Fig. 5. Lineweaver-Burk plots of α-glucosidase inhibition in the presence of: A) **1**; B) **11**; C) **22**; D) **26**; E) **27**, and of α-amylase inhibition in the presence of: F) **1**; G) **11**; H) **27**. Plotted data are means ± SD (n = 3).

Table 4
Kinetic parameters for α-glucosidase and α-amylase inhibition.[a]

compound	α-Glu			α-Amy	
	Type of inhibition	$K_i = \pm$ SD (μM)	$K'_i = \pm$ SD (μM)	Type of inhibition	$K_i = \pm$ SD (μM)
Acarbose	competitive	185.1 ± 18.4	–	competitive	25.1 ± 1.14
1	non-competitive	79.1 ± 2.0	–	competitive	12.7 ± 3.0
11	non-competitive	146.2 ± 5.7	–	competitive	29.9 ± 2.4
22	mixed-type	234.2 ± 7.2	44.2 ± 5.4	–	–
26	non-competitive	125.0 ± 5.1	–	–	–
27	mixed-type	42.0 ± 2.3	4.9 ± 0.2	competitive	8.5 ± 0.9

[a] K_i refers to the constants for the formation EI complex; K'_i refers to the constants for the formation ESI complex.

allosteric site. Into this allosteric binding site, **22** interacts with His258 through a π-π stacking interaction, whereas **27** interacts with the cavity through a H-bond interaction between the OH group at C-2 and Arg269, whereas the B-ring is involved in a π-cation interaction with Lys12 and a π-π interaction with His258. No other significant interactions were found with other reported allosteric sites (sitescore < 1, see Tables S1 and S2) for both molecules. These data suggest that compounds **22** and **27**, aside from exhibiting compatibility with the catalytic site (Section 2.6), demonstrate a high affinity for the most likely allosteric site identified. This observation agrees with the findings from the kinetic assays.

The analysis of the kinetics data for the α-amylase inhibition pointed out the two more active inhibitors, **11** and **27**, as well as the obovatol (**1**), as competitive inhibitors. Furthermore, the K_i values (**11**: 29.9 μM; **27**: 8.5 μM; **1**: 12.7 μM) are in good agreement with the experimental IC_{50} values (**11**: 12.7 μM; **27**: 6.2 μM; **1**: 23.6 μM), and docking findings (**11**: −4.83 Kcal/mol; **27**: −5.50 Kcal/mol; **1**: −4.48 Kcal/mol), with **27** being the most effective inhibitor toward α-amylase, as well as toward α-glucosidase.

2.5. *Intrinsic fluorescence measurements*

The affinity of the most effective inhibitors (**11**, **22**, **26** and **27**) for α-Glu and α-Amy was determined spectroscopically by a fluorescence quenching experiment. Analogous experiments were performed on obovatol (**1**) for comparison. Tryptophan (Tyr) possesses a chromophore group that is responsible for the endogenous fluorescence of most proteins, among which α-glucosidase and α-amylase are examples [56]. The interaction between the enzyme and its substrate modifies the microenvironment of Trp residues, thus producing a decrease in fluorescence. More specifically, α-Glu displays an intrinsic fluorescence emission peak at 340 nm when excited at 295 nm. Similarly, α-Amy shows an emission peak at nearly 345 nm when excited ad 295 nm. In Fig. 6, the fluorescence spectra of α-Glu in the presence of increasing concentrations of **1**, **11**, **22**, **26**, and **27** are reported. Fig. 7 shows the spectra of α-Amy in the presence of increasing concentrations of **1**, **11**, and **27**. These measurements were performed at 298.15, 303.15, and 310.15 K to get more information on the nature of the interaction. The addition of the tested compounds progressively reduced the fluorescence intensity of both enzymes. Compound **22** exhibits an intrinsic fluorescence in the region at 415 nm when it is irradiated at 295 nm (Fig. S15). Therefore, the fluorescence spectra of α-Glu in the presence of increasing concentrations of **22** show a double peak (Fig. 6). The data recorded were elaborated according to the equation (4). The linearity of Stern-Volmer plots indicated a single mode of quenching for the two enzymes (Figs. 8-9). From these plots, and according to the equation, the dissociation constant K_{sv} and the bimolecular quenching constant K_q were determined. These data are collected in Table 5. From the analysis, the same behaviors can be observed for all compounds with α-glucosidase and α-amylase. The increasing temperature causes an increasing number of collisions with the consequent raising of K_{sv} values. Thus, the fluorescence quenching occurs through a dynamic mechanism. The number of binding sites (n) and the binding constant (K_a) for the interaction of the neolignan-type ligands with α-glucosidase and α-amylase were calculated using equation (5) (Eq. (5), and these values are reported in Table 5. In the temperature range studied, the number of binding sites n was close to 1 for all the tested compounds against both enzymes, suggesting the formation of a one-to-one complex between the fluorophore and the quencher. Looking at the obtained K_a values, compound **27** shows the greatest affinity for both enzymes, corroborating all the results therein reported.

2.6. *Circular dichroism*

Circular dichroism (CD) spectroscopy is mainly used to monitor the secondary structure (α-helix, β-sheet, β-turn and random coil) changes of proteins in solution and, more specifically, the conformational changes of a given protein in the presence of selected ligands [57,58]. CD measurements were carried out to have further confirmation of the interaction of obovatol (**1**) and its analogues with the higher activities (**1**, **11**, **22**, **26**, and **27**) towards α-glucosidase, thus providing details and valuable information regarding the inhibition process. We have not obtained reliable results using α-amylase owing to experimental conditions that were not suitable for CD measurement.

The CD measurement of the α-Glu enzyme was carried out in the absence and presence of different aliquots of the selected compounds. ECD spectra were acquired in the 200–260 nm range and are reported in Fig. 10. α-Glu had a high percentage of α-helix structures that exhibited two negative bands around 210 and 222 nm, attributable to n → π* transition for the peptide bond of α-helix structures as reported in the literature [45,59]. The ECD spectra of **1**, **11**, **22**, **26** and **27** in buffer solutions in the absence of enzyme were acquired as well. As expected, since the compounds are not chiral, they do not show any CD signal in the absorption region (Fig. 10, orange line). Then, ECD spectra of the α-Glu solution with increasing amounts of ligands were recorded. All reported spectra of α-Glu change after the addition of ligands; the intensity of both bands observed in the spectrum of α-Glu decreases, indicating the loss of part of the α-helix structures as a result of the interaction of the tested compounds with α-Glu. In order to visualize these differences, we subtracted the spectra of α-Glu in the presence of ligands minus the spectra of α-Glu. The resulting CD difference spectra (inset in Fig. 10) clearly show that CD spectroscopy can detect the conformational changes of α-Glu induced by interaction with the tested compounds. In particular, all difference spectra show a negative band below 210 nm and a positive band centered at around 225 nm (inset in Fig. 10). These spectroscopic features of the ECD spectra resemble that observed for the random coil conformation. Indeed, the random coil is characterized by a positive contribution at about 220 nm, a negative band at about 200 nm and a cross over point in the 210 nm region. However, a positive contribution at 225 nm is also observed for β-turns, together with a positive signal in the 200 nm region. Therefore, the broad positive feature of the difference spectra suggests that the content of random coil and β-turns may increase after the interaction with the tested compounds. CD data were further estimated with the secondary structure estimation software included in the JASCO Spectra Manager software to quantify the changes in the secondary structure (Table S3 in

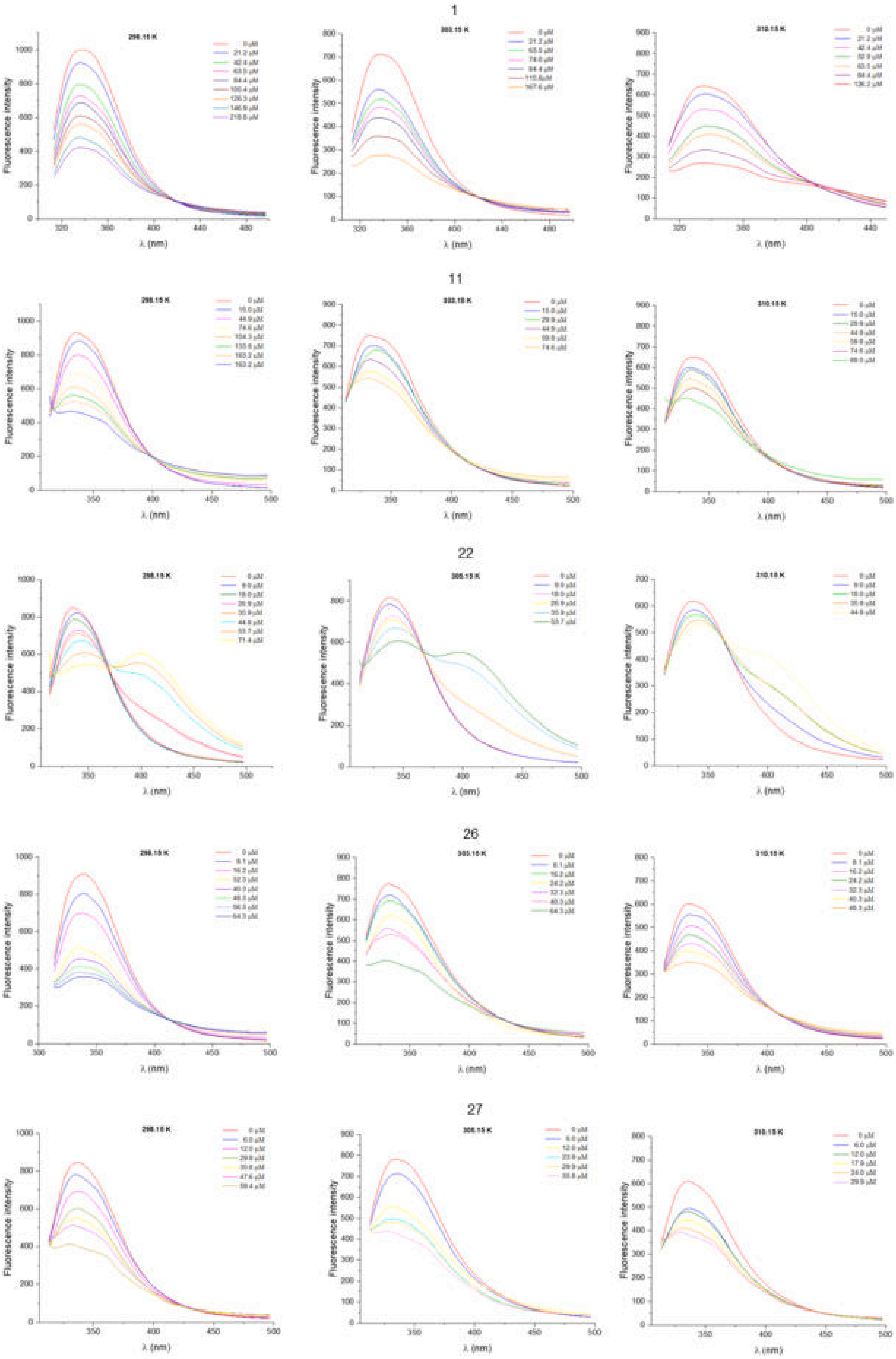

Fig. 6. Changes in the intrinsic α-Glu fluorescence at different concentrations of **1**, **11**, **22**, **26** and **27** and different temperatures (pH 6.9, λex = 295 nm).

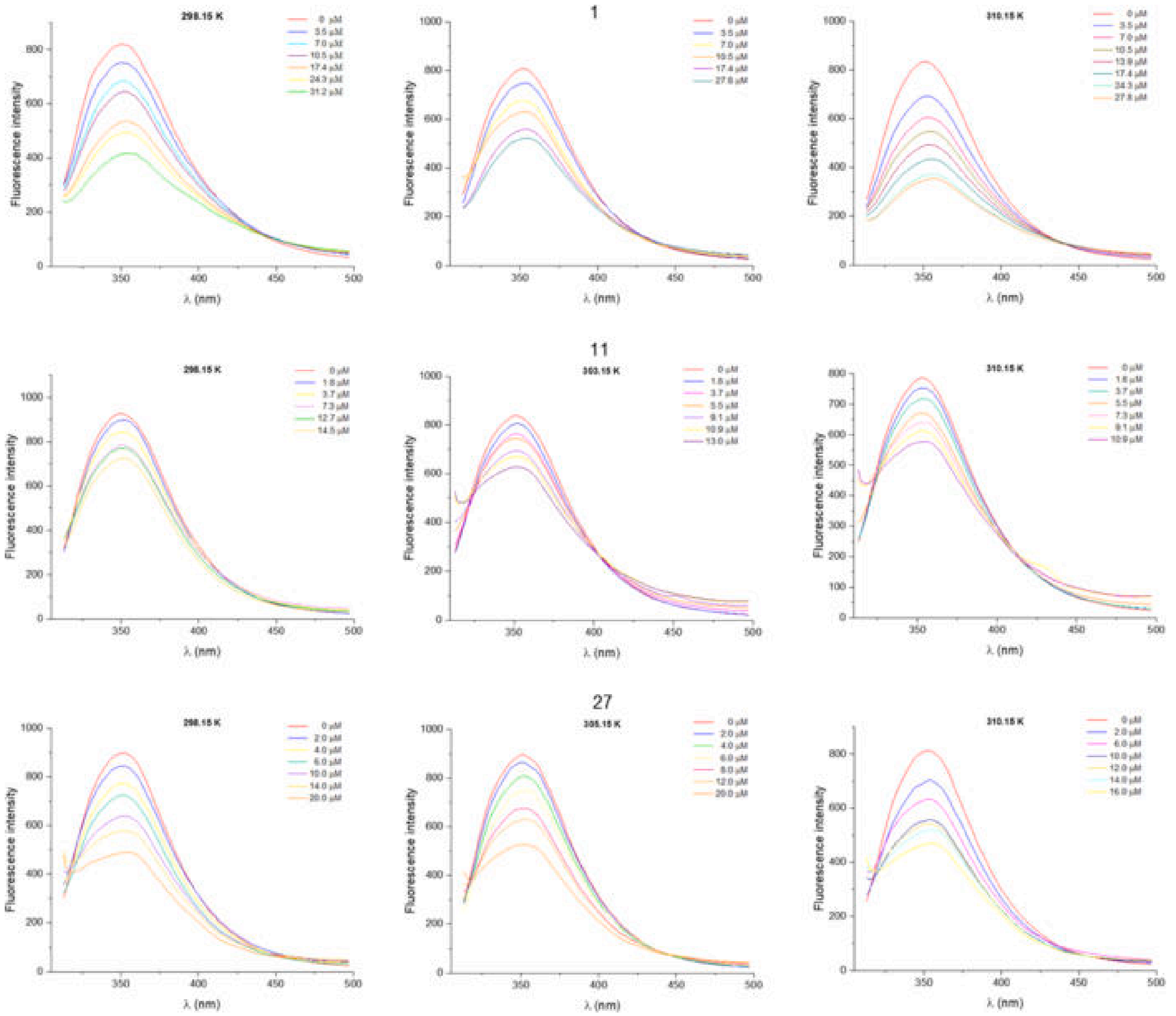

Fig. 7. Changes in the intrinsic α-Amy fluorescence at different concentrations of **1**, **11** and **27** at different temperatures (pH 6.9, λex = 295 nm).

Supplementary material). According to the data, it was observed that the interaction between the α-Glu and all tested compounds (**1**, **11**, **22**, **26** and **27**) caused a significant decrease of α-helix content at the highest concentration of employed inhibitor. The α-helix content exhibited an approximate percentage decrease from 38 % to 27 %. The interaction of all compounds also resulted in an increase in random coil content as evidenced by the difference spectra between the enzyme/neolignan complexes at ratios of 1:1 (0.5: 0.5 μM) and 1:6 (0.5: 3.0 μM) minus the CD spectrum of α-Glu. Additionally, **1**, **11** and **22** caused an increase in β-sheet content with the increase of the complex ratio, while compounds **26** and **27** led to an initially increase at a 1:1 ratio and a decrease at a ratio 1:6. Other notable differences have been shown in β-turn content where **1**, **26** and **27** exhibited a slight increase while **11** and **22** showed a reduction.

2.7. Surface plasmon resonance imaging

SPR imaging (SPRI) is an extremely versatile technique for the multiplexed detection of biomolecular interactions with high sensitivity [60]. It uses optical detectors for spatial monitoring of localized differences in the reflectivity of the incident light (Δ%R), which can be seen as brighter or darker regions in the SPR image, from an array of biomolecules linked to chemically modified gold surface [61]. Label-free and real-time analyses can be carried out with high throughput and low sample consumption by coupling microfluidic devices with the SPRI apparatus [62]. We used SPRI to obtain further evidence of the interaction between compounds (**1**, **11**, **22**, **26**, and **27**) and α-glucosidase and α-amylase. To this aim, we immobilized the enzymes on the gold surface of the SPR sensor through the amine-coupling reaction between *N*-hydroxysuccinimidyl (NHS) ester ends of Dithiobis(N)succinimidyl-propionate (DTSP)-modified gold surface and the *N*-terminal groups of the enzymes. These coupling conditions are typically carried out in a buffered solution close to physiological ambient and, therefore, should not alter the inherent activity of the biomolecules by preserving their structure [63]. Fig. 11 shows representative SPRI curves for the enzyme immobilization, kept at the lowest density possible, the same for both enzymes, to give a proper kinetic signal, minimizing mass transport, steric hindrance, crowding and aggregation typically associated with high-capacity surface [64]. The deactivation of excess NHS reactive groups on the surface was obtained by a solution of Trizma solution (0.1

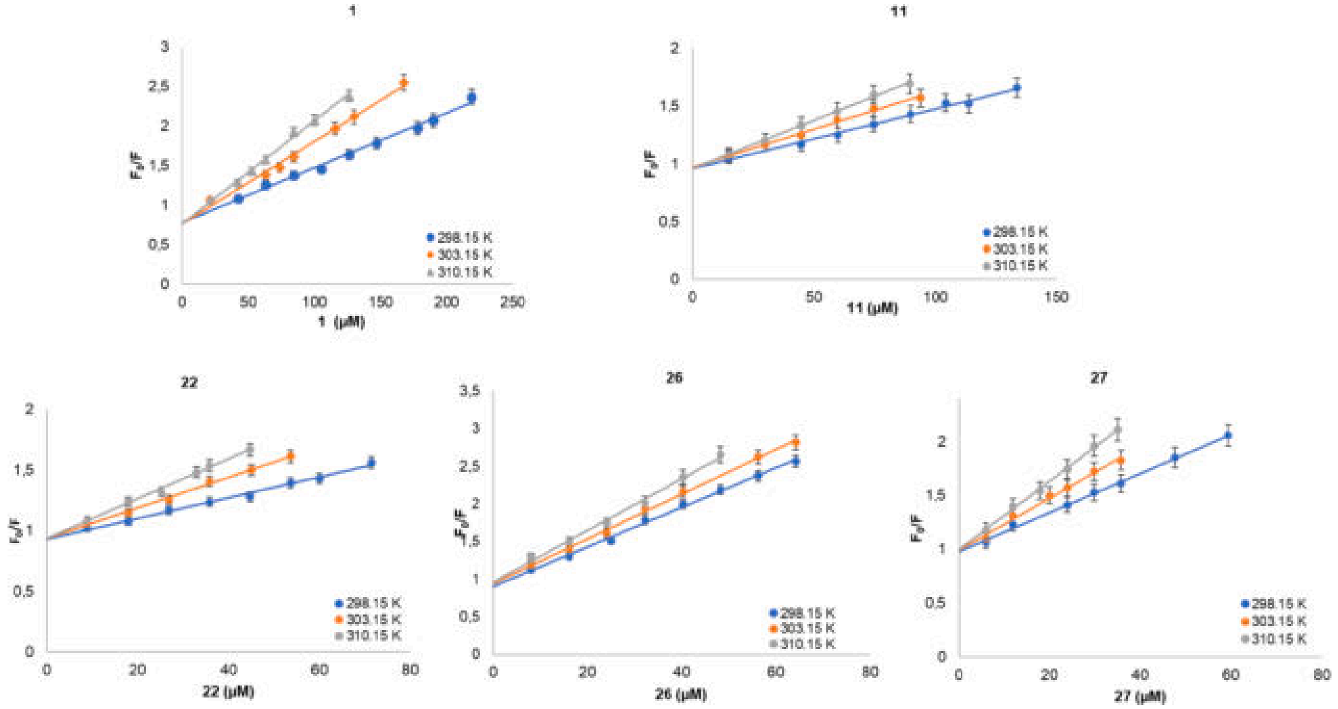

Fig. 8. Stern-Volmer plots for the quenching effects of α-Glu with selected compounds (**1**, **11**, **22**, **26** and **27**).

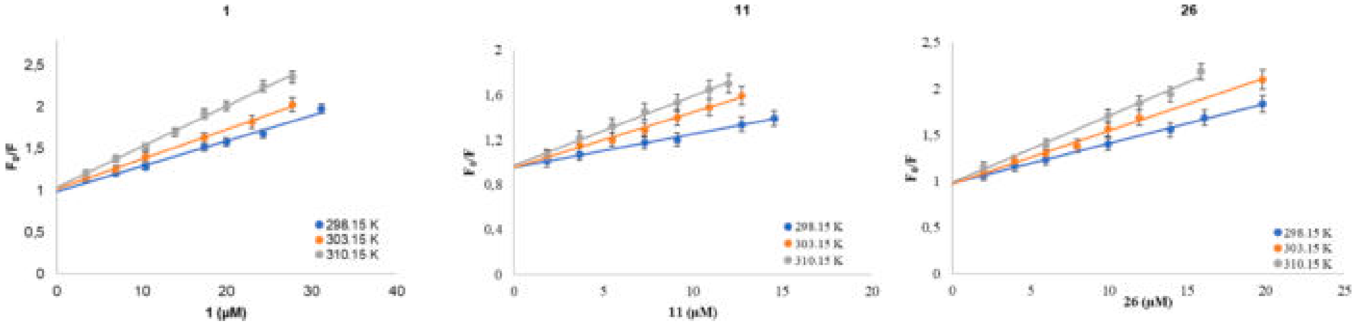

Fig. 9. Stern-Volmer plots for the quenching effects of α-Amy with selected compounds (**1**, **11** and **27**).

M in water) for at least 10 min.

Different concentrations of **1**, **11**, **22**, **26** and **27** were tested and the level of binding of the neolignans to the immobilized α-Amy and α-Glu was measured based on the change of the SPRI response in Δ%R values obtained in each microchannel and recorded as the real-time profile of the SPRI response versus time. Fig. S16 shows representative SPRI changes in percent reflectivity (Δ%R) over time detected for the interaction of α-Amy and the new analogues (**1, 11** and **27**) using their 200, 400 and 800 µM solutions in PBS. The larger SPRI shift detected for the interaction between **27** and α-Amy provided evidence of the capacity of the compound to interact with the α-Amy preferentially compared to **11** and **1**. Assuming one-to-one binding model, the rate and affinity constants can be easily calculated, when the association and dissociation curves are measured for various analyte concentrations [65]. The association and dissociation rate constants (K_a, K_d) and the affinity constant, calculated as $K_D = K_d/K_a$, were determined by exponential fit of the association and dissociation phase performed with Origin software using the theoretical equations reported in Supplementary material. The kinetic parameters are given in Table 6. The smaller the K_D value, the greater the binding affinity of the ligand for its target. As shown in Fig. S16 and Table 6, the results suggested that **27** have high binding ability to α-amylase. The binding order of new compounds for α-Amy is **27** > **11** > **1**, suggesting that the binding affinity was much more affected by the presence of bromine atoms and the thioether link than by the number of hydroxyl groups. To understand whether such an interaction is related to the molecular structure of the neolignan derivatives, acarbose was used as control. Acarbose is a pseudo-tetrasaccharide with high number of hydroxyl gropus whose structural differences may have greater effects on the binding ability. (Fig. S16). In this case, the exponential fitting fails to estimate kinetic parameters. The higher K_D value ($0.78 \pm 0.12 \text{ x}10^{-3}$M) reported in the literature for the acarbose interaction with α-Amy is very likely caused by the differences in its structure compared to new anologues which is expected to have different steric requirements. Therefore, the binding ability between the three compounds (**1**, **11**, and **27**) and α-amylase was significantly higher than the acarbose and enzyme.

Fig. S17 shows representative SPRI changes in percent reflectivity (Δ%R) over time detected for the interaction of α-Glu and the new analogues (**1**, **11**, **22**, **26** and **27**). As shown in Fig. S17 and Table 7, also in this case, the compounds bound to immobilized α-Glu in a concentration-dependent manner, and the K_D values were calculated to be in the range $10^{-4} \div 10^{-6}$. The binding order of new analogues for α-Glu is **27** > **26** > **22** > **11** > **1**, confirming that new neolignans bound to α-Glu and α-Amy formed new stable complexes that exhibited fast

Table 5

Quenching constants K_{sv}, quenching rate constants K_q and binding constants K_a of the interaction of obovatol (**1**) and its analogues (**11**, **22**, **26,** and **27**) with α-Glu and/or α-Amy.

	T (K)	K_{sv} ($\times 10^4$ L/mol)	K_q ($\times 10^{12}$ L/mol)	R^2	K_a ($\times 10^4$ L/mol)	n	R^2
α-Glu							
1	298.15	0.70 ± 0.02	0.70 ± 0.02	0.9905	0.95 ± 0.04	1.11	0.9954
	303.15	1.04 ± 0.15	1.04 ± 0.15	0.9902	1.79 ± 0.23	0.76	0.9936
	310.15	1.30 ± 0.18	1.30 ± 0.18	0.9935	2.20 ± 0.32	1.35	0.9994
11	298.15	0.54 ± 0.02	0.54 ± 0.02	0.9942	0.20 ± 0.14	1.18	0.9933
	303.15	0.70 ± 0.03	0.70 ± 0.03	0.9931	0.24 ± 0.04	1.14	0.9951
	310.15	0.84 ± 0.04	0.84 ± 0.04	0.9980	0.52 ± 0.05	1.20	0.9935
22	298.15	0.81 ± 0.02	0.81 ± 0.02	0.9908	0.20 ± 0.02	1.36	0.9902
	303.15	1.27 ± 0.45	1.27 ± 0.45	0.9929	0.35 ± 0.08	1.28	0.9902
	310.15	1.64 ± 0.38	1.64 ± 0.38	0.9989	0.50 ± 0.04	1.30	0.9926
26	298.15	2.61 ± 0.25	2.61 ± 0.25	0.9976	0.99 ± 0.13	1.23	0.9965
	303.15	2.96 ± 0.15	2.96 ± 0.15	0.9973	1.84 ± 0.24	1.11	0.9978
	310.15	3.33 ± 0.18	3.33 ± 0.18	0.9925	2.18 ± 0.31	1.11	0.9972
27	298.15	1.81 ± 0.34	1.81 ± 0.34	0.9940	2.09 ± 0.44	0.96	0.9932
	303.15	2.42 ± 0.18	2.42 ± 0.18	0.9912	3.54 ± 0.57	0.96	0.9908
	310.15	3.18 ± 0.21	3.18 ± 0.21	0.9965	3.87 ± 0.62	0.83	0.9919
α-Amy							
1	298.15	3.03 ± 0.40	3.03 ± 0.40	0.9902	3.49 ± 0.70	0.95	0.9944
	303.15	3.62 ± 0.14	3.62 ± 0.14	0.9978	4.53 ± 0.54	0.93	0.9930
	310.15	4.89 ± 0.21	4.89 ± 0.21	0.9962	6.30 ± 0.54	0.92	0.9966
11	298.15	2.95 ± 0.29	2.95 ± 0.29	0.9934	1.70 ± 0.12	1.14	0.9929
	303.15	4.89 ± 0.32	4.89 ± 0.32	0.9913	2.25 ± 0.04	0.90	0.9994
	310.15	6.32 ± 0.13	6.32 ± 0.13	0.9907	6.10 ± 0.37	1.00	0.9924
27	298.15	4.25 ± 0.04	4.25 ± 0.04	0.9985	3.10 ± 0.22	1.11	0.9926
	303.15	5.75 ± 0.36	5.75 ± 0.36	0.9941	4.78 ± 0.54	1.07	0.9923
	310.15	7.20 ± 0.23	7.20 ± 0.23	0.9904	7.60 ± 0.07	0.97	0.9942

binding and slow dissociation reaction, as well as strong binding.

2.8. Biological activity and cytotoxicity

The biological activity of the most active neolignan analogues (**11**, **22**, **26** and **27**) were tested toward HCT-116 colon cancer cell line under a phase-contrast microscope, after 24 h of treatment, with respect to obovatol (**1**). Cells were treated with ½ IC_{50}, IC_{50} and 2 × IC_{50} concentrations for α-Glu inhibition of each compound, and compared to untreated control cells (Fig. 12). No differences were detected for **26** and **27** treated cells, suggesting that these α-glucosidase inhibitors were non toxic at these concentrations. A significant reduction of cell number, cellular shrinkage and detachment from the adjacent cells was recorded for **1**, **11** and less pronounced for **22** treated cells, especially when cells were treated with 2 × IC_{50} concentrations for α-Glu inhibition. Morphological changes were also detected after staining with acridine orange and ethidium-bromide (AO/EB). AO can penetrate into the living cells and emits green fluorescence, while EB enters the cells after cell membrane damage and emits red fluorescence. As shown in Fig. 13, untreated viable cells emitted green fluorescence due to the AO staining of both cytoplasm and nuclei. No condensed chromatin was detected in all treated cells with IC_{50} concentration for α-Glu inhibition. Interestingly, cells treated with **27** are similar to untreated cells, confirming no cytotoxicity effect of this compound at this concentration. The AO staining in the cytoplasm of other treated cells was detectable as bright punctate dots, revealing acidic compartments, such as lysosomes and vacuole, namely acidic vesicular organelles (AVOs). These features represent the hallmark of non-apoptotic cell death, such as autophagy. Autophagy is characterized by sequestration of cellular organelles and proteins into autophagic vesicles and fusion of these vesicles with lysosomes. In cancer cells autophagy plays a dual role to either suppress early carcinogenesis or support the survival and growth of advanced tumors. The vitro cytotoxicity of obovatol (**1**), **11**, **22**, **26** and **27** was additionally tested by MTT assay, after 24 h of exposure. IC_{50} was defined as the concentration of the compound inhibiting cell survival rate by 50 %, compared with a vehicle-treated control cells. The IC_{50} values of tested compounds are shown in Fig. 14. Compared to obovatol (**1**), all tested analogues showed a cytotoxic activity (IC_{50}) against HCT-116 cell line. The most active was compound **26** with the IC_{50} value of 97 ± 11 μM. The cytotoxic activities of these compounds are considered moderate, but in consideration of their inhibitory activity (IC_{50}) towards α-Amy and α-Glu, compound **27** could be consider safe, while the compound **11** could be consider as antiproliferative. Based on the obtained results, these compounds can serve as promising hit compounds for further bioactivity optimization and anti–type 2 diabetes study.

3. Conclusions

The present work reports efficient synthesis tactics based on either the Ullmann coupling reaction or a thia-Michael addition reaction to produce obovatol (**1**) and a set of ten new analogues within the neolignan class. This study presents, for the first time, a comprehensive assessment of the α-glucosidase and α-amylase inhibitory activities of **1** and its analogues with the purpose of evaluating new scaffolds for type 2 diabetes drug research. Our investigation demonstrated promising inhibitory activities for the naturally occurring compound **1** and the

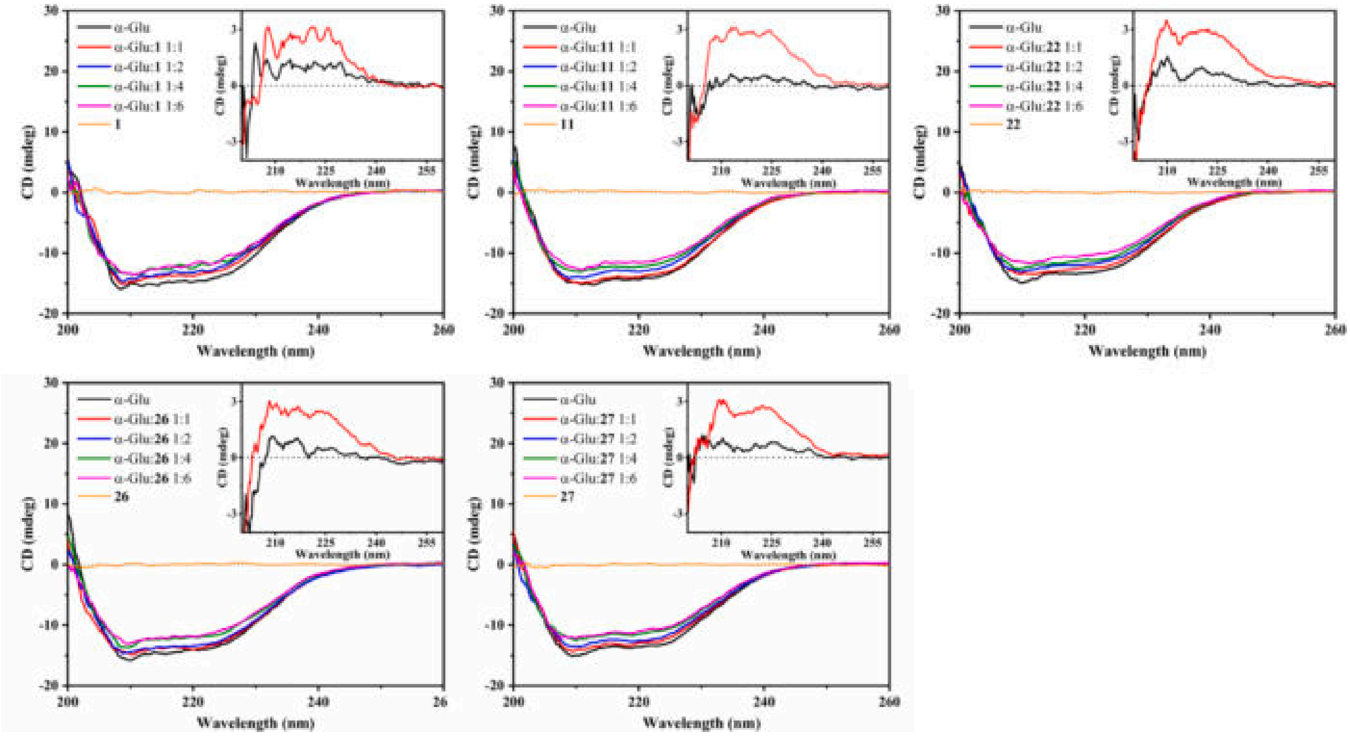

Fig. 10. ECD spectra of α-Glucosidase [0.5 μM] in the presence of increasing amounts of **1**, **11**, **22**, **26** and **27**. Orange line represents the spectra of the relative compound at the concentration of 3 μM in the absence of the enzyme. Inset: CD difference between the spectra of α-Glu/compound 1:1 complex minus that of α-Glu alone (black line) and of α-Glu/compound 1:6 complexes minus that of α-Glu alone (red line). (For interpretation of the references to colour in this figure legend, the reader is referred to the web version of this article.)

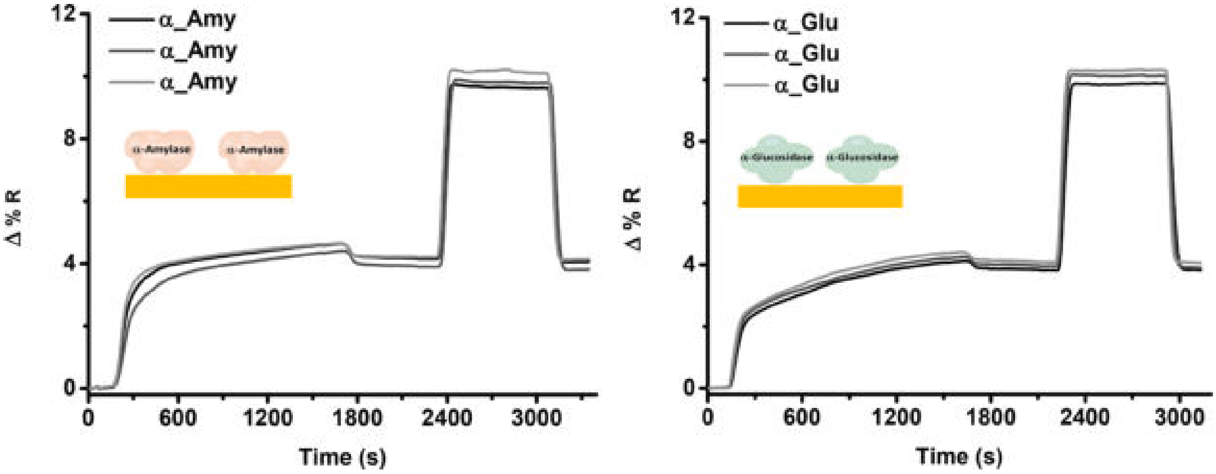

Fig. 11. Representative changes in percent reflectivity (Δ%R) over time detected for the immobilization of the enzymes α-Amy (280 μg mL^{-1} in PBS) and α-Glu (130 μg mL^{-1} in PBS). The curves shown refer to independent immobilizations performed in parallel through the channels of the microfluidic device in contact with the modified gold surface of the SPRI, followed by the deactivation step with Trizma solution to block unreacted NHS ester moieties.

Table 6
Kinetic parameters obtained for the interaction of three neolignans (**1, 11** and **27**) with α-amylase immobilized onto the gold surface of the SPRI sensor.

α-Amy/Compound	K$_a$(mol^{-1}·L·s^{-1})	K$_d$(s^{-1})	K$_D$(M)
1	7.04 ± 0.66	1.66 ± 0.12 x10^{-4}	2.36 ± 0.02 x10^{-5}
11	3.41 ± 0.17	4.21 ± 0.15 x10^{-5}	1.23 ± 0.04 x10^{-5}
27	3.62 ± 0.19	3.02 ± 0.09 x10^{-5}	8.34 ± 0.03 x10^{-6}
Acarbose[a]	11.12 ± 0.07	8.8 ± 0.04 x10^{-3}	0.78 ± 0.12 x10^{-3b}

Values are expressed as means ± standard errors obtained from experiments performed at three different concentrations. [a]Kinetic parameters available from the literature for acarbose and α-amylase interaction[b] [66].

newly synthesized analogues **11**, **22**, **26**, and **27**. To better understand the enzymatic inhibition outcomes, an *in silico* evaluation of these neolignans was conducted to assess their affinity for the enzymatic catalytic sites. The *in silico* data revealed favorable interactions between obovatol and its analogues with both enzymes, underscoring how the combined influence of free hydroxyl groups and the presence of bromine atoms enhances inhibitory activity not only in the ether **11** but also in the thioether derivative **27**. Conversely, the presence of allyl chains in the diaryl ether structures was not a crucial structural feature for inhibitory activity.

Kinetic results indicated different modes of α-Glu inhibition by the most promising active neolignans despite their very similar structures

Table 7
Kinetic parameters obtained for the interaction of three neolignans (**1, 11, 22, 26** and **27**) with α-glucosidase immobilized onto the gold surface of the SPRI sensor.

α-Glu/Compound	k_a($mol^{-1}·L·s^{-1}$)	k_d(s^{-1})	K_D(M)
1	2.83 ± 0.23	1.24 ± 0.01 x10^{-3}	4.38 ± 0.003 x10^{-4}
11	6.22 ± 0.28	1.17 ± 0.06 x10^{-3}	1.88 ± 0.01 x10^{-4}
22	7.75 ± 0.72	7.33 ± 0.39 x10^{-4}	9.46 ± 0.05 x10^{-5}
26	7.56 ± 0.26	2.14 ± 0.95 x10^{-4}	2.83 ± 0.13 x10^{-5}
27	5.52 ± 0.16	3.14 ± 0.35x10^{-5}	5.69 ± 0.06 x10^{-6}

Values are expressed as means ± standard errors obtained from experiments performed at three different concentrations.

with **1**, **11** and **26** acting as non-competitive inhibitors and **22** and **27** as mixed-type inhibitors. In contrast, α-Amy inhibition occurred through the same mechanism for all the compounds acting as competitive inhibitors. Compounds **22** and **27** exhibited mixed-type inhibition behaviours towards α-Glu, and additional docking studies supported their compatibility with both the catalytic and allosteric sites, in agreement with the kinetic data. Fluorescence data confirmed dynamic interactions between enzymes and neolignans, while CD results suggested conformational changes in α-Glu induced by increasing amounts of neolignans. SPRI measurements demonstrated that all of the compounds were better ligands than acarbose and exhibited strong binding to α-amylase and α-glucosidase, providing scientific support for the screening of these analogues as potential inhibitors. Interestingly, the evaluation of their biological activity using the IC_{50} concentration (inhibitory activity towards α-Glu) on HCT-116 colon cancer cell line, suggests that obovatol (**1**), **11**, **22** and **26** are able to induce a programmed cell death, through the activation of autophagic pathway, while no effect was detected when cells were treated with **27**. Moreover, based on their cytotoxic effect and inhibitory activity for α-Glu, the neolignane and analogues we tested can be considered safe (**27**), borderline (**26**) or with anti-proliferative activity (**1**, **11**, **22**).

This comprehensive study indicates that the neolignane obovatol (**1**) and its analogues **11**, **22**, **26** and, mostly **27**, represent promising compounds with interesting structural features for developing a novel hypoglycemic drug for treating type-2 diabetes. Future perspectives will concern the validation of the inhibitory activity of the synthesized compounds towards human enzymes, the assessment of their mechanism of action and *in vivo* analyses.

4. Experimental

4.1. General

All reactions were carried out under nitrogen or argon atmosphere using dry solvents under anhydrous conditions, unless otherwise noted. Solvents for chromatographic purification (ethyl acetate, cyclohexane, *n*-hexane, acetone, dichloromethane, methanol) were purchased at the highest commercial quality. Reagents were purchased at the highest commercial quality and used without further purification, unless otherwise noted. Evaporations were conducted under reduced pressure at 35 °C unless otherwise noted. Yields refer to chromatographically and spectroscopically (^{1}H NMR) homogeneous materials, unless otherwise noted. Reactions were monitored by thin-layer chromatography (TLC) carried out using pre-coated Merck silica gel plates 60F-254. Merck silica gel (60, particle size 40–63 μm) was used for column chromatography. The visualization of the reaction components was obtained under UV light at a wavelength of 254 nm. NMR spectra were recorded on Bruker DPX-300 and Bruker Avance I 300 MHz spectrometers and were calibrated using residual undeuterated solvent signals as internal references [$CDCl_3$ (^{1}H): $\delta = 7.26$ ppm; $CDCl_3$ (^{13}C): $\delta = 77.0$ ppm]. The following abbreviation were used to describe the multiplicities: s for singlet, d for doublet, dd for double doublet, dt for double triplet, dq for double quartet brs for broad singlet, ddt for double double triplet, dddt for double double double, m for multiplet. IR spectra were recorded between 4000 and 450 cm^{-1} on a Bruker IFS55 (OPUS/IR 3.0.2) FT-IR spectrometer. High resolution mass spectrometry (HRMS) was performed using the Electro Spray Ionization (ESI) method. The α-glucosidase (α-Glu) and α-amylase (α-Amy) inhibition assays and kinetic measurements were performed on a 96-well microplate and the Synergy H1 microplate reader was used.

4.2. Chemical synthesis

4.2.1. 2-(allyloxy)-3-bromophenol (5)

The commercially available 3-bromobenzene-1,2-diol (300.0 mg, 1.58 mmol) was dissolved in dry acetone (12 mL) and K_2CO_3 (219.4 mg, 1.59 mmol) was added. This mixture was stirred at room temperature for 10 min, after which time allyl bromide (268.8 mg, 2.22 mmol) was added, and this reaction mixture was refluxed for 2 h. The mixture was cooled down to room temperature, diluted with ethyl acetate (5 mL), filtered and evaporated. The resulting oily residue was purified by silica gel column chromatography (*n*-hexane → *n*-hexane/ethyl acetate 98:2) to afford compound **5** (224.7 mg, 62 %) as a yellowish oil. IR (NaCl): 3450, 2925, 1717, 1459, 1252 cm^{-1}; ^{1}H NMR (300 MHz, $CDCl_3$): δ 7.09 (dd, $J = 6.4$, 3.2 Hz, 1H, H-5), 6.94–6.88 (m, 2H, H-4/H-6), 6.22–5.98 (m, 1H, H-8), 5.47 (dq, $J = 17.1$, 1.5 Hz, 1H, H_a-9), 5.36 (dq, $J = 10.3$, 1.5 Hz, 1H, H_b-9), 4.60 (dt, $J = 6.0$, 1.2 Hz, 2H, H-7); ^{13}C NMR (75 MHz, $CDCl_3$): δ 150.4 (C-2), 143.3 (C-1), 132.8 (C-8), 126.0 (C-4), 124.6 (C-5), 119.7 (C-9), 116.1 (C-3), 114.9 (C-6), 74.6 (C-7); HRMS (neg. ESI) calcd for $C_9H_8O_2Br$ $[M-H]^+$: 226,9713, found 226,9711.

4.2.2. 5-allyl-3-bromobenzene-1,2-diol (6)

A 1 M Et_2AlCl solution in *n*-hexane (1.96 mL, 1.96 mmol) was added dropwise to a solution of **5** (224.7 mg, 0.98 mmol) in dry CH_2Cl_2 (1 mL). The mixture was stirred at room temperature for 3 h, after which time 2 N aqueous HCl (2 mL) was added at 0 °C. The mixture was partitioned using CH_2Cl_2 (2 × 5 mL), and the combined organic layers were washed with water, dried oved anhydrous Na_2SO_4, filtered and evaporated. The resulting residue was purified by silica gel column chromatography, eluting with cyclohexane → cyclohexane/acetone (85:15), to furnish the expected Claisen-Cope product **6** (179.6 mg, 80 %) as a brownish oil. IR (NaCl): 3439, 2925, 1721, 1441, 1069 cm^{-1};^{1}H NMR (300 MHz, $CDCl_3$): δ 6.97 (d, $J = 2.1$ Hz, 1H, H-4), 6.67 (d, $J = 2.0$ Hz, 1H, H-6), 5.95 (m, 1H, H-8), 5.14–5.03 (m, 2H, H-9), 3.31 (dt, $J = 7.4$, 1.3 Hz, 2H, H-7). ^{13}C NMR (75 MHz, $CDCl_3$): δ 144.3 (C-1) 142.0 (C-2), 136.9 (C-8), 136.5 (C-8), 134.3 (C-5), 123.2 (C-4), 116.3 (C-9), 115.4 (C-6), 113.8 (C-3), 39.3 (C-7).; HRMS (neg. ESI) calcd for $C_9H_8O_2Br$ $[M-H]^+$: 226,9713, found 226,9710.

4.2.3. General procedure for methylation reactions

To a solution of **6** or **20** (1 eq.) in DMF was added K_2CO_3 (2 eq.). After stirring for 30 min, methyl iodide (3 equiv. per OH group) was added, and the resulting mixture was stirred for 4 h at room temperature. The reaction mixture was then quenched by addition of saturated aqueous NH_4Cl (2 mL) and diluted with diethyl ether (4 mL), further extracted with diethyl ether (2 × 5 mL) and the combined organic layers were washed with brine, dried over anhydrous Na_2SO_4, filtered and evaporated.

4.2.4. 5-allyl-1-bromo-2,3-dimethoxybenzene (7)

According to the above general procedure, the reaction of **6** (112.3 mg, 0.49 mmol) with potassium carbonate (135.6 mg, 0.98 mmol) and methyl iodide (208.7 mg, 1.47 mmol) gave a crude residue, which was purified by silica gel column chromatography, eluting with *n*-hexane → *n*-hexane/acetone (98:2), to afford compound **7** (88.2 mg, 70 %) as a yellowish oil. ^{1}H NMR (300 MHz, $CDCl_3$): δ 6.97 (d, $J = 1.9$ Hz, 1H, H-4), 6.67 (d, $J = 1.9$ Hz, 1H, H-6), 6.04–5.83 (m, 1H, H-8), 5.16–5.05(m, 2H, H-9), 3.85 (s, 3H, CH_3), 3.83 (s, 3H, CH_3), 3.31 (dt, $J = 6.7$, 1.4 Hz, 2H, H-7). ^{13}C NMR (75 MHz, $CDCl_3$): δ 153.6 (C-3), 144.7 (C-2), 137.3 (C-8),

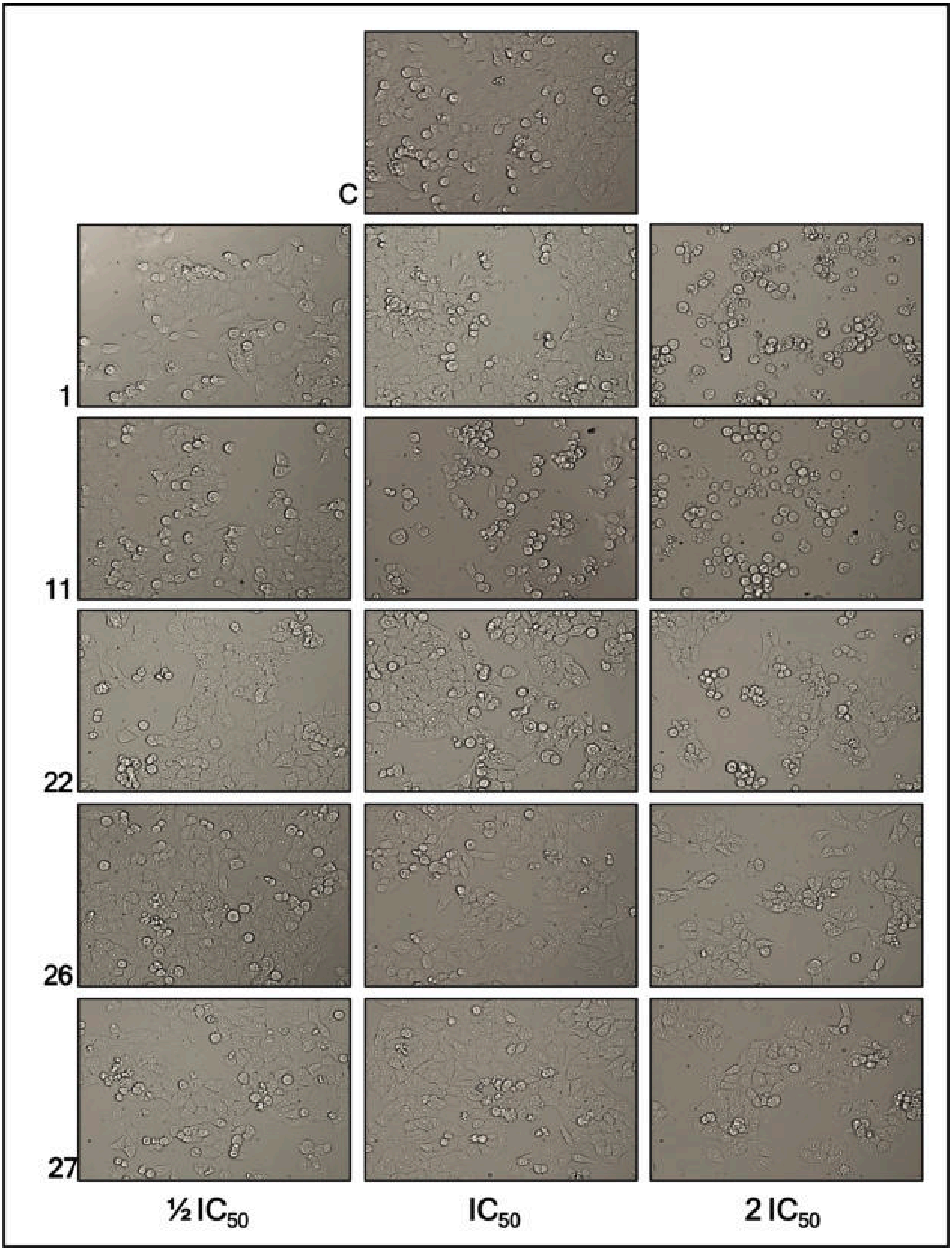

Fig. 12. Inverted phase-contrast micrographs of HCT-116 cells treated for 24 h with ½ IC_{50}, IC_{50} and 2 × IC_{50} concentrations for α-Glu inhibition of **1**, **11**, **22**, **26** and **27**. Magnification 200 × .

136.6 (C-5), 124.5 (C-6), 117.5 (C-4), 116.5(C-8), 112.1(C-1), 60.6 (CH_3), 56.0 (CH_3), 39.7 (C-7). Spectroscopic data were in agreement with those previously reported [67].

4.2.5. 5-bromo-2-methoxybenzaldehyde (21)

According to the general procedure, the reaction of commercially available 5-bromo-2-hydroxybenzaldehyde **20** (130.0 mg, 0.75 mmol) with potassium carbonate (207.5 mg, 1.5 mmol) and methyl iodide (320.0 mg, 2.25 mmol) furnished a crude residue, which was purified by

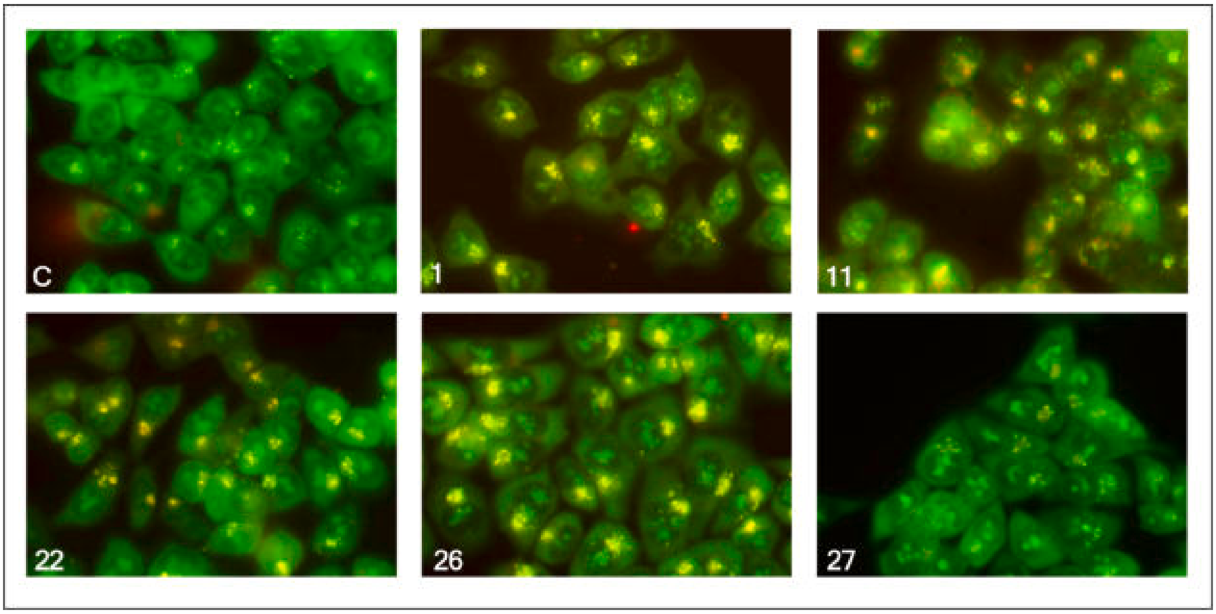

Fig. 13. Fluorescence micrographs of HCT-116 cells treated for 24 h with ½ IC_{50}, IC_{50} and 2 × IC_{50} concentrations for α-Glu inhibition of **1**, **11**, **22**, **26** and **27** after AO/EB double staining. Untreated cells display green fluorescence of both cytoplasm and nuclei. In the cytoplasm of **1**, **11**, **22** and **26** are visible bright punctate dots, namely acidic vesicular organelles (AVOs), a hallmark of autophagic cell death. Magnification 630 × . (For interpretation of the references to colour in this figure legend, the reader is referred to the web version of this article.)

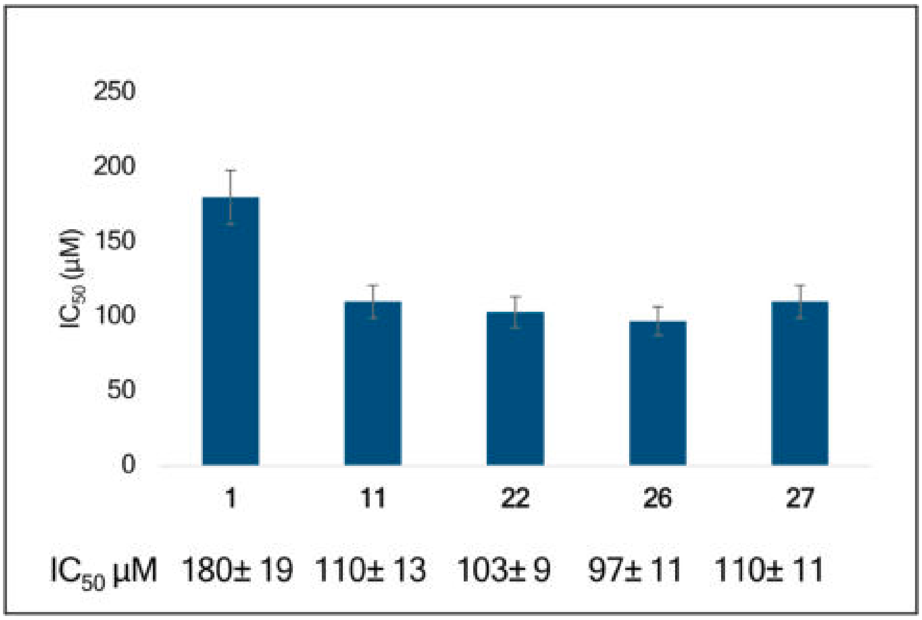

Fig. 14. IC_{50} values (concentration that inhibit the 50 % of cell proliferation compared to untreated cells) obtained from the dose–response model, expressed as μM ± SD (standard deviation). Experiments were performed in triplicate.

silica gel column chromatography, eluting with cyclohexane/acetone (95:5), to afford compound **21** (155.4 mg, 97 %) as a yellow solid. ^{1}H NMR (300 MHz, $CDCl_3$): δ 10.38 (s, 1H, H-7), 7.92 (d, *J* = 2.6 Hz, 1H, H-6), 7.63 (dd, *J* = 8.9, 2.6 Hz, 1H, H-2), 6.90 (d, *J* = 8.9 Hz, 1H, H-3), 3.90 (s, 3H, CH_3). Spectroscopic data were in agreement with those previously reported [68].

4.2.6. General procedure for Ullmann coupling reactions

A mixture of bromide (1 eq.), *p*-allylphenol (1.5 eq.), Cs_2CO_3(2 eq.), CuI (10 mol%) and *N,N*-dimethylglycine hydrochloride (30 mol%) in dioxane (2 mL) was heated at 90 °C under nitrogen in a sealed tube for 48 h, after which time the reaction mixture was cooled down to room temperature and partitioned between ethyl acetate (4 mL) and water (4 mL). The organic layer was separated, and the aqueous layer was further extracted with ethyl acetate (3 × 5 mL). The combined organic layers were washed with brine, dried over Na_2SO_4, filtered and evaporated.

4.2.7. 4-allyl-6-(4′-allylphenoxy)-1,2-dimethoxybenzene (9)

According to the above general procedure, the reaction of the bromide **7** (65.0 mg, 0.25 mmol) with the *p*-allylphenol **8** (50 mg, 0.38 mmol) gave a crude residue, which was purified by silica gel column chromatography, eluting with *n*-hexane → *n*-hexane/acetone (98:2), to afford compound **9** (38.8 mg, 52 %) as a yellowish oil. IR (NaCl): 2920, 2848, 1508, 1426, 1234, 1094 cm^{-1}; ^{1}H NMR (300 MHz, $CDCl_3$): δ 7.11

(d, J = 8.7 Hz, 2H, H-2′/H-6′), 6.90 (d, J = 8.7 Hz, 2H, H-3′/H-5′), 6.54 (d, J = 2.0 Hz, 1H, H-5), 6.42 (d, J = 2.0 Hz, 1H, H-3), 5.92 (dddt, J = 17.5, 16.1, 10.7, 6.7 Hz, 2H, H-8 /H-8′), 5.17–4.96 (m, 4H, H-9/H-9′), 3.88 (s, 3H, CH$_3$), 3.81 (s, 3H, CH$_3$), 3.35 (d, J = 6.7 Hz, 2H, H-7), 3.27 (d, J = 6.7 Hz, 2H, H-7′). ^{13}C NMR (75 MHz, CDCl$_3$): δ 156.2 (C-1′), 153.8 (C-2), 149.6 (C-6), 139.2 (C-1), 137.7(C-8′), 137.1 (C-8), 136.0 (C-5′), 134.3(C-4), 129.7 (C-3′/C-5′), 117.5 (C-2′/C-6′), 116.1 (C-9′), 115.7 (C-9), 113.4 (C-3), 108.2 (C-5), 61.1 (CH$_3$), 56.2 (CH$_3$), 40.1 (C-7), 39.5 (C-7′); HRMS (pos. ESI) calcd for $C_{20}H_{23}O_3$ [M + H]$^+$: 311.1647, found 311.1630.

4.2.8. 3-allyl-6-(4′-allylphenoxy)-1-methoxybenzene (14)

According to the general procedure, the reaction of the bromide **13** (50.0 mg, 0.25 mmol) with the *p*-allylphenol **12** (61.8 mg, 0.38 mmol) gave a crude residue, which was purified by silica gel column chromatography, eluting with *n*-hexane → *n*-hexane/acetone (98:2), to afford compound **14** (64.4 mg, 94 %) as a colourless oil. IR (NaCl): 3077, 2977, 2836, 1638, 1613, 1597, 1503, 1463, 1417, 1271, 1225, 1151, 1036 cm^{-1}; ^{1}H NMR (300 MHz, CDCl$_3$): δ 7.12 (d, J = 8.7 Hz, 2H, H-2′/H-6′), 6.93–6.87 (m, 3H, H-3′/H-5′, H-5), 6.85 (d, J = 2.1 Hz, 1H, H-2), 6.75 (dd, J = 8.1, 2.1 Hz, 1H, H-4), 6.00 (dddt, J = 17.1, 10.3, 8.6, 6.7 Hz, 2H, H-8/H-8′), 5.20–5.04 (m, 4H. H-9/H-9′), 3.85 (s, 3H, CH$_3$), 3.41 (dt, J = 6.7, 1.5 Hz, 2H, H-7), 3.37 (dt, J = 6.7, 1.5 Hz, 2H, H-7′).^{13}C NMR (75 MHz, CDCl$_3$): δ 156.5 (C-1′), 151.3 (C-2), 143.5 (C-1), 137.7 (C-8′), 137.3 (C-8), 136.7 (C-4′), 133.9 (C-4), 129.6 (C-3′/C-5′), 121.0 (C-5), 120.8 (C-6), 117.2 (C-2′/C-6′), 116.0 (C-9′), 115.7 (C-9), 113.2 (C-3), 56.0 (CH3), 40.0 (C-7), 39.5 (C-7′). HRMS (pos. ESI): calcd for $C_{19}H_{20}O_2Na$ [M + Na]$^+$: 303.1361, found 303.1345.

4.2.9. 1-(6-(4′-allyl-2′-methoxyphenoxy)-4-methoxyphenyl)acetic acid (17)

According to the general procedure, the reaction of **16** (170.0 mg, 0.70 mmol) with **12** (172.4 mg, 1.05 mmol) gave a crude residue, which was purified by silica gel column chromatography, cyclohexane/ethyl acetate (95:5) → cyclohexane/ethyl acetate (70:30), to afford compound **17** (90.0 mg, 40 %) as a colourless oil. IR (NaCl): 2993, 1765, 1379.07, 1244, 1056, 750 cm^{-1}; ^{1}H NMR (300 MHz, CDCl$_3$): δ 7.17 (d, J = 8.3 Hz, 1H, H-2), 6.88 (d, J = 8.1 Hz, 1H, H-6′), 6.79 (d, J = 2.0 Hz, 1H, H-4′), 6.72 (dd, J = 8.1, 2.0 Hz, 1H, H-5′), 6.56 (dd, J = 8.3, 2.5 Hz, 1H, H-3), 6.24 (d, J = 2.5 Hz, 1H, H-5), 6.08 – 5.88 (m, 1H, H-8′), 5.18 – 5.02 (m, 2H, H-9′), 3.77 (s, 3H, CH$_3$), 3.75 (s, 2H, H-7), 3.69 (s, 3H, CH$_3$), 3.37 (dt, J = 6.7, 1.5 Hz, 2H, H-7′). ^{13}C NMR (75 MHz, CDCl$_3$): δ 176.9 (C-8), 160.1 (C-4), 157.1 (C-2′), 151.2 (C-6), 142.7 (C-1′), 137.3 (C-9′), 137.2 (C-4′), 131.6 (C-2), 121.3 (C-1), 121.0 (C-5′), 116.0 (C-8′), 115.7 (C-6′), 113.2 (C-3′), 107.1 (C-3), 102.8 (C-5), 55.9 (CH$_3$), 55.4 (CH$_3$), 40.7 (C-7′), 35.1(C-7). HRMS (neg. ESI): calcd for $C_{19}H_{19}O_5$ [M + H]$^-$: 327.12332, found 327.1236.

4.2.10. 6-(4′-allyl-2′-methoxyphenoxy)-benzoic acid (19)

According to the general procedure, the reaction of **18** (100.0 mg, 0.46 mmol) with **12** (113.3 mg; 0.69 mmol) afforded a crude residue, which was purified by silica gel column chromatography, eluting with cyclohexane/ethyl acetate (95:5), to afford compound **19** (20 mg, 20 %) as an orange solid. IR (NaCl): 2924, 2854, 1685, 1610, 1597, 1504, 1463, 1423, 1273, 1232, 1161, 1122, 1035 cm^{-1}; ^{1}H NMR (300 MHz, CDCl$_3$): δ 8.03 (d, J = 9.1 Hz, 2H, H-2/H-4), 7.01 (d, J = 8.0 Hz, 1H, H-6′), 6.92 (d, J = 9.0 Hz, 2H, H-1/H-5), 6.85 (d, J = 2.0 Hz, 1H, H-3′), 6.81 (dd, J = 8.0, 2.0 Hz, 1H, H-5′), 6.00 (ddt, J = 17.0, 10.3, 6.7 Hz, 1H, H-8′), 5.24–5.08 (m, 2H, H-9′), 3.78 (s, 3H, CH$_3$), 3.42 (dd, J = 6.7, 1.5 Hz, 2H, H-7′). ^{13}C NMR (75 MHz, CDCl$_3$): δ 171.6 (C-7), 163.2 (C-6), 151.5 (C-2′), 141.3 (C-1′), 138.5 (C-8′), 137.1(C-4′), 132.3 (C-2/C-4), 122.8 (C-3), 122.3 (C-5′), 121.2 (C-6′), 116.3 (C-9′), 115.7 (C-1/C-5), 113.3 (C-3′), 55.9 (CH$_3$), 40.1 (C-7′). HRMS (neg. ESI) calcd for $C_{17}H_{15}O_4$ [M + H]$^-$: 283.0970, found 283.0969.

4.2.11. 6-(4′-allylphenoxy)-3-methoxybenzaldehyde (22)

According to the general procedure, the reaction of **21** (155.4 mg, 0.72 mmol) with **12** (145.0 mg, 1.08 mmol) gave a crude residue, which was purified by silica gel column chromatography, eluting with CH$_2$Cl$_2$, to afford compound **22** (110.0 mg, 52 %) as an orange oil. IR (NaCl):3360, 3076, 2922, 2852., 1683,1639, 1613, 1505, 1488, 1425, 1393, 1266, 1219, 1151, 1025, 819 cm^{-1}; ^{1}H NMR (300 MHz, CDCl$_3$): δ 10.40 (s, 1H,H-7), 7.43 (d, J = 3.1 Hz, 1H, H-1), 7.22 (dd, J = 9.0, 3.2 Hz, 1H, H-5), 7.11 (d, J = 8.7 Hz, 2H, H-2′/H-6′), 6.94 (d, J = 9.0 Hz, 1H, H-4), 6.86 (d, J = 8.6 Hz, 2H, H-3′/H-5′), 5.94 (ddt, J = 16.0, 10.7, 6.7 Hz, 1H, H-8′), 5.18 – 5.03 (m, 2H, H-9′), 3.89 (s, 3H, CH$_3$), 3.34 (dt, J = 6.8, 1.6 Hz, 2H, H-7′). ^{13}C NMR (75 MHz, CDCl$_3$): δ 189.4 (C-7), 158.1 (C-3), 155.8 (C-1′), 151.1 (C-6), 137.5 (C-8′), 135.1 (C-4′), 130.0 (C3′/C-5′), 127.0 (C-3), 125.5 (C-5), 118.4 (C-2′/C-6′), 118.0 (C-1), 115.9 (C-9′), 113.2 (C-4), 56.2 (CH$_3$), 39.5 (C-7′). HRMS (pos. ESI): calcd for $C_{17}H_{16}O_3Na$ [M + Na]$^+$: 291.0997, found 291.0980.

4.2.12. General procedure for demethylation reactions

To a solution of an Ullman coupling product (1.0 eq.) in dry CH$_2$Cl$_2$ at –78 °C was added BBr$_3$ (1 M solution in CH$_2$Cl$_2$, 1.0 or 2.0 eq.), and the reaction mixture was stirred for 2 h, after which time it was quenched by an addition of methanol (1 mL) and diluted with ethyl acetate (2 mL). The mixture was extracted with ethyl acetate (3 × 5 mL) and the combined organic layers were washed with brine, dried over Na$_2$SO$_4$, filtered and evaporated.

4.2.13. 4-allyl-6-(4′-allylphenoxy)-benzene-1,2-diol (1)

According to the general procedure, the reaction of **9** (65.0 mg, 0.21 mmol) with BBr$_3$ (1 M solution in CH$_2$Cl$_2$, 0.44 mmol) gave a crude residue, which was purified by silica gel column chromatography, eluting with CH$_2$Cl$_2$, to afford obovatol (**1**, 50 mg, 84 %) as a yellowish oil. IR (NaCl): 3450, 2924, 2853, 1639, 1602, 1504, 1444, 1360, 1214, 1168, 1022 cm^{-1}; ^{1}H NMR (300 MHz, CDCl$_3$): δ 7.18 (d, J = 8.6 Hz, 2H, H-2′/H-6′), 6.97 (d, J = 8.6 Hz, 2H, H-3′/H-5′), 6.60 (d, J = 1.9 Hz, 1H, H-3), 6.31 (d, J = 1.9 Hz, 1H, H-5), 6.01–5.77 (m, 2H, H-7/H-7′), 5.35 (brs, 1H, OH), 5.30 (brs, 1H, OH), 5.22–4.92 (m, 4H, H-9/H-9′), 3.40 (dt, J = 6.8, 1.5 Hz, 2H, H-7), 3.23 (d, J = 6.7, 1.6 Hz, 2H, H-7′). ^{13}C NMR (75 MHz, CDCl$_3$): δ 155.0 (C-1′), 144.8 (C-6), 143.7 (C-2), 137.4 (C-8), 137.2 (C-8′), 135.3 (C-4′), 132.9 (C-1), 132.5 (C-4), 129.9 (C-3′/C-5′), 117.9(C-2′/C-6′), 115.9 (C-9), 115.8 (C-9′), 111.1 (C-3), 110.6 (C-5), 39.7 (C-7), 39.4 (C-7′). HRMS (neg. ESI): calcd for $C_{18}H_{17}O_3$ [M + H]$^-$:281.1178, found 281.1176.

4.2.14. 4-allyl-6-(4′-allylphenoxy)-2-methoxyphenol (10)

According to the general procedure, the reaction of **9** (30.0 mg, 0.10 mmol) with BBr$_3$ (1 M solution in CH$_2$Cl$_2$, 0.1 mmol) afforded compound **10** (28.7 mg, 97 %) as a brownish oil. IR (NaCl): 2923, 2853, 1504, 1452, 1433, 1222, 1084 cm^{-1}; ^{1}H NMR (300 MHz, CDCl$_3$): δ 7.12 (d, J = 8.5 Hz, 2H, H-2′/H-6′), 6.92 (d, J = 8.6 Hz, 2H, H-3′/H-5′), 6.53 (d, J = 1.9 Hz, 1H, H-5), 6.44 (d, J = 1.8 Hz, 1H, H-3), 6.10–5.80 (m, 2H, H-8/H-8′), 5.14–4.99 (m, 4H, H-9/H-9′), 3.91 (s, 3H, CH$_3$), 3.36 (dt, J = 6.5, 1.6 Hz, 2H, H-7), 3.26 (dt, J = 6.6, 1.5 Hz, 2H, H-7′).^{13}C NMR (75 MHz, CDCl$_3$): δ 155.8 (C-1′), 147.9 (C-2), 143.3 (C-6), 143.0, 137.6 (C-8′), 137.3 (C-8), 135.6 (C-4′), 134.5 (C-4), 131.5 (C-1), 129.7(C-3′/C-5′), 117.3 (C-2′/C-6′), 115.9 (C-9), 115.7 (C-9′), 113.0 (C-5), 107.3 (C-3), 56.3(CH$_3$), 39.9 (C-7), 39.5 (C-7′). HRMS (pos. ESI): calcd for $C_{19}H_{21}O_3$ [M + Na]$^+$: 319.1310, found 319.1302.

4.2.15. 4-(8-bromopropyl)-6[4′-(8′-bromopropyl)phenoxy)]benzene-1,2-diol (11)

To a solution of the Ullmann coupling **9** (30.0 mg, 0.10 mmol) in dry CH$_2$Cl$_2$ (0.2 mL) at –78 °C was added BBr$_3$ (1 M solution in CH$_2$Cl$_2$, 0.1 mmol). After stirring for only 30 min at the same temperature, the reaction mixture was allowed to warm up to room temperature and stirred for 2 h, after which time it was quenched by an addition of methanol (1 mL) and diluted with ethyl acetate (2 mL). The mixture was extracted with ethyl acetate (3 × 5 mL) and the combined organic layers were washed with brine, dried over Na_2SO_4, filtered and evaporated. The resulting crude residue was purified by silica gel column chromatography, eluting with cyclohexane/acetone (90:10) → cyclohexane/acetone (80:20), to afford compound **11** (22.5 mg, 50 %) as a brownish oil. IR (NaCl): 3425, 2923, 1505, 1219, 1170, 601 cm^{-1}; ^1H NMR (300 MHz, $CDCl_3$): δ 7.18 (d, $J = 8.4$ Hz, 2H, H-2′/H-6′), 6.97 (d, $J = 8.4$ Hz, 2H, H-3′/H-5′), 6.59 (d, $J = 1.9$ Hz, 1H, H-3), 6.33 (d, $J = 1.8$ Hz, 1H, H-5), 4.45–3.94 (m, 2H, H-8/H-8′), 3.29–2.76 (m, 4H, H-7/H-7′), 1.68 (dd, $J = 19.6$, 6.6 Hz, 6H, CH_3). ^{13}C NMR (75 MHz, $CDCl_3$): δ 155.6 (C-1′), 144.9 (C-2), 143.3 (C-6), 133.8 (C-1), 133.7 (C-4), 131.0 (C-4′), 130.7 (C-2′/C-6′), 117.7 (C-3′/C-5′), 111.9 (C-5), 111.6 (C-3), 46.9 (C-7), 46.6 (C-7′), 43.6 (C-8), 43.6 (C-8′), 25.7 (CH_3), 25.6 (CH_3). HRMS (neg. ESI) calcd for $C_{18}H_{19}Br_2O_3$ $[M + H]^-$: 442.9857, found 442. 9681.

4.2.16. 4-allyl-6-(4′-allylphenoxy) phenol (15)

According to the general procedure, the reaction of **14** (30.0 mg, 0.11 mmol) with BBr_3 (1 M solution in CH_2Cl_2, 0.11 mmol) afforded **15** (28.4 mg, 97 %) as a brownish oil. IR (NaCl): 3520, 3077, 2923, 2853, 1637, 1598, 1502, 1452, 1432, 1270, 1223, 1163, 1111 cm^{-1}; ^1H NMR (300 MHz, $CDCl_3$): δ 7.17(d, $J = 8.6$ Hz, 2H, H-2′/H-6′), 6.97 (d, $J = 8.6$ Hz, 2H, H-3′/H-5′), 6.92 (d, $J = 2.1$ Hz, 1H, H-2), 6.83(d, $J = 8.3$ Hz, 1H, H-5), 6.69 (dd, $J = 8.3$, 2.1 Hz, 1H, H-4), 6.26–5.74 (m, 2H, H-8/H-8′), 5.34–4.91 (m, 4H, H-9/H-9′), 3.38 (ddd, $J = 8.6$, 6.8, 1.6 Hz, 4H, H-7/H-7′). ^{13}C NMR (75 MHz, $CDCl_3$): δ 155.3 (C-1′), 147.3 (C-1), 141.8 (C-6), 137.4 (C-3), 137.3 (C-4′), 136.9 (C-8), 135.2 (C-8′), 129.9(C-3′/C-5′), 120.6 (C-2′/C-6′), 118.7 (C-4), 117.8 (C-3), 116.2(C-9), 116.0 (C-9′), 115.9 (C-2), 39.7 (C-7), 39.4 (C-7′). HRMS (neg. ESI) calcd for $C_{18}H_{17}O_2$ $[M + H]^-$: 265.1229, found 265.1233.

4.2.17. General procedure for 2-methoxyphenol oxidation and thia-Michael addition

To a stirred suspension of SIBX (2.15 eq.) in dry THF (*ca* 0.05 M) was added the 2-methoxyphenol (1.0 eq.). After stirring in the dark at room temperature for 16 h, the thiophenol (3.0 eq.) was added and the reaction mixture was stirred at room temperature for 2 h. The white suspension was filtered out from the reaction mixture. The filter cake was washed with CH_2Cl_2 (20 mL), and the combined filtrate and washings were poured into water (30 mL). After separation, the aqueous layer was further extracted with CH_2Cl_2 (30 mL) and the combined organic layers were washed with saturated aqueous $NaHCO_3$ (4 × 15 mL) and treated with saturated aqueous $Na_2S_2O_4$ (2 mL) for 10 min with vigorous shaking under nitrogen in the dark. The resulting solution was washed with water (10 mL), brine (10 mL), dried over Na_2SO_4, filtered and evaporated.

4.2.18. 4-allyl-6-(phenylthio)- benzene-1,2-diol (26)

According to the general procedure, the reaction of the 2-methoxyphenol **12** (50.0 mg, 0.30 mmol) with the thiophenol **24** (99.2 mg, 0.90 mmol) gave a crude residue, which was purified by silica gel column chromatography, eluting with cyclohexane → cyclohexane/ethyl acetate (80:20), to afford compound **26** (45 mg, 45 %) as a colourless oil. IR (NaCl):3422, 3073.72, 2923, 2853, 1581.91, 1638.35, 1581, 1478, 1438, 1265, 1168, 1122, 988, 737, 688 cm^{-1}; ^1H NMR (300 MHz, $CDCl_3$): δ 7.33 (d, $J = 8.4$ Hz, 2H, H-3′/H-5′), 7.28–7.24 (m, 1H, H-4′), 7.19 (dd, $J = 8.3$, 1.4 Hz, 2H, H-2′/H-6′), 7.00 (d, $J = 2.0$ Hz, 1H, H-5), 6.97 (d, $J = 2.0$ Hz, 1H, H-3), 6.21–5.79 (m, 1H, H-8), 5.28–5.05 (m, 2H, H-9), 3.38 (dt, $J = 6.7$, 1.5 Hz, 2H, H-7). ^{13}C NMR (75 MHz, $CDCl_3$): δ 144.2 (C-2), 142.8 (C-1), 137.1 (C-7), 135.8 (C-1′), 133.5 (C-4), 129.3 (C-2′/C-6′), 127.3 (C-4′), 126.9 (C-3′/C-5′), 126.2 (C-5), 118.0 (C-9), 116.1 (C-3), 115.9 (C-6), 39.4 (H-7). HRMS (neg. ESI) calcd for $C_{15}H_{13}O_2S$ $[M + H]^-$: 257.0636, found 257.0639.

4.2.19. 4-allyl-6-((4′-bromophenyl) thio)-benzene-1,2-diol (27)

According to the general procedure, the reaction of **12** (100.0 mg, 0.60 mmol) with the thiophenol **25** (346.0 mg, 1.80 mmol) gave a crude residue, which was purified by silica gel column chromatography, eluting with cyclohexane → cyclohexane/ethyl acetate (95:5), to afford compound **27** (70 mg, 35 %) after flash column chromatography, eluting with cyclohexane → cyclohexane: ethyl acetate 95:5. colourless oil. IR (NaCl): 3420., 2923, 2853, 1715, 1471, 1267, 668 cm^{-1}; ^1H NMR (300 MHz, $CDCl_3$): δ 7.35 (d, $J = 8.7$ Hz, 2H, H-3′/H-5′), 6.94 (d, $J = 8.7$ Hz, 2H, H-2′/H-6′), 6.88 (d, $J = 1.8$ Hz, 1H, H-3), 6.19 (d, $J = 1.8$ Hz, 1H, H-5), 6.03–5.79 (m, 1H, H-8), 5.16–5.00 (m, 1H, H-9), 3.29 (dt, $J = 6.7$,1.5 Hz, 2H, H-7). ^{13}C NMR (75 MHz, $CDCl_3$): δ 144.4 (C-2), 142.9 (C-1), 137.1 (C-8), 135.2 (C-1′), 133.8 (C-5), 132.4 (C-3′/C-5′), 128.5 (C-2′/C-6′), 127.3 (C-5), 120.0 (C-4′), 118.3 (C-9), 116.3 (C-3), 115.5 (C-6), 39.4 (C-7). HRMS (neg. ESI) calcd for $C_{15}H_{14}BrO_2S$ $[M + H]^+$: 336.9798, found 336.9718.

4.3. Assay and kinetic of α-glucosidase inhibition

The α-glucosidase inhibition assay was performed using the conditions previously reported [47]. Briefly, in a 96-well microplate, the α-glucosidase solution (0.25 U/ml in 50 mM phosphate buffer, pH 6.8; 100 μl) was mixed with different aliquots (2, 4, 6, 8 μl) of tested compounds (stock solutions in methanol ranging from 3.22 mM to 0.5 mM). Then, the substrate *p*-nitrophenyl-α-glucoside (NPG, 78 μM, 100 μl) was added and the microplate was incubated at 37 °C for 30 min under shaking. The reaction was stopped by adding 1 M aqueous Na_2CO_3 (10 μl) and the absorbance of *p*-nitrophenol was measured at 405 nm with the Synergy H1 microplate reader (BioTek, Bad Friedrichshall, Germany). Acarbose was used as a reference standard. The assays were performed in triplicate with different concentrations for each compound. The amount of methanol used in the experiment did not affect the glucosidase inhibitory activity. The inhibition percentage was calculated by the following equation:

$$\%inhibition = \frac{OD_{\text{control}} - OD_{\text{sample}}}{OD_{\text{control}}} * 100 \tag{1}$$

where, OD_{control} represents the measured optical density for the enzyme-substrate mixture in the absence of inhibitor, and OD_{sample} represents the optical density of the reaction mixture in the presence of the inhibitor. The concentration required to inhibit the 50 % activity of the enzyme (IC_{50}) was calculated by regression analysis. The results of the *in vitro* assay are reported in Table 3 as IC_{50} values. The mode of inhibition and the inhibitory constants for obovatol (**1**) and the most promising analogues were determined similarly. Precisely, mixtures containing α-Glu (5 μL of a 31 μM solution), the inhibitors (**1**: 0, 62.5, 125.0, 190.0 μM; **11**: 0, 60.0, 120.0, 168.0 μM; **22**: 0, 30.0, 67.0, 120.0 μM; **26:** 0, 27.5, 56.0, 82.5 μM; **27**: 0, 20.0, 40.0, 60.0 μM) and NPG at different concentration (2.00, 1.50, 1.25, 0.83, 0.50, 0.33 and 0.15 mM) were incubated at 37 °C and the optical density was read at 405 nm every 1 min for 30 min with the Synergy H1. The initial velocity (ν) was determined as the slope of the OD changes at 405 nm during the linear course of the reaction. The inhibition constants were calculated from the equations:

$$v_0 = \frac{v_{\max} S}{K_{\text{m}}\left(1 + \frac{I}{K_{\text{i}}}\right) + S} \tag{2}$$

$$v_0 = \frac{v_{\max} S}{K_{\text{m}}\left(1 + \frac{I}{K_{\text{i}}}\right) + S\left(1 + \frac{I}{K'_{\text{i}}}\right)} \tag{3}$$

where ν_0 is the initial velocity in the absence and presence of the inhibitor, S and I are the concentrations of substrate and inhibitor, respectively, ν_{max} is the maximum velocity, Km is the Michaelis-Menten constant, K_i is the competitive inhibition constant, and K'_i is the uncompetitive inhibition constant. The graphs of slope and y-intercept of Lineweaver-Burk plots versus the inhibitor concentration gave a straight line, whose intercept corresponds to K_i and K'_i values, respectively.

4.4. Assay and kinetic of α-amylase inhibition

The inhibition of the porcine pancreatic α-amylase (EC3.2.1.1, Type VI-B, α-Amy) was performed as previously reported [45]. The reactions were carried out in test tubes by mixing 50 μL of the enzyme solution (6 U/ml in 20 mM phosphate buffer containing 6.7 mM NaCl) with tested compounds (2, 4, 6, 8 of 3.87–0.50 mM solutions). The reactions were incubated at 37 °C for 10 min, then, a starch solution (0.5 % in phosphate buffer; 50 μL), previously stirred at 90 °C for 20 min, was added in the test tubes, and the mixtures were incubated again at 37 °C for 15 min. Lastly, 100 μL of a 96 mM 3,5-dinitrosalicylic acid solution (containing 30 % sodium potassium tartrate in 2 N NaOH) were added, and the test tubes were heated at 80 °C for 10 min. Each mixture was diluted with water (final volume 540 μL) and the solutions were moved into a 96-well microplate, and the OD at 540 nm was acquired. Acarbose was used as a positive reference. The inhibition percentage was calculated by solving Eq. (1); the IC_{50} values were calculated by regression analysis of inhibition % data. The mode of inhibition and the kinetic parameters for obovatol (**1**) and the most promising analogues were determined according to a procedure previously described with some modifications. The assay was performed in 96-well microplates (final volume of 200 μL). In a typical set of experiments were added 10 μL of α-Amy solution (4.0 U/mL in 0.1 mM phosphate buffer containing 0.02 % NaN_3; pH 6.8) and the inhibitor at different concentrations (**1**: 0, 8.0, 16.0, 24.0 μM; **11**: 0, 15.0, 25.0, 50.0 μM; **27**: 0, 3.0, 6.0, 18.0 μM). The plate was incubated at 37 °C for 10 min, and the reaction was started by addition of different aliquots of 10 mM 2-chloro-4-nitrophenyl-α-maltotrioside (CNPG3; 1.25, 1.00, 0.75, 0.50, 0.25 mM), the OD was measured at 405 nm every minute for 30 min, maintaining the plate at 37 °C. The initial velocity (ν) was determined as the slope of the OD changes at 405 nm during the linear course of the reaction. The data acquired were elaborated according to the Lineweaver-Burk equations (Eq. 2–3).

4.5. Fluorescence measurement

Fluorescence experiments were performed as previously reported [45]. A solution of α-Glu (0.03 mg/mL in 0.1 M phosphate buffer containing 0.1 M NaCl, pH 6.9; 2 mL) or α-Amy (0.4 mg/mL in 0.1 M phosphate buffer containing 0.1 M NaCl, pH 6.9; 2 mL) was titrated by consecutive additions (2 or 4 μL) respectively of **1**, **11**, **22**, **26** or **27** for glucosidase and **1**, **11**, or **27** for amylase. The concentration of starting solution of the tested compounds was chosen based on the IC_{50} values. Each titration was replicated three times at 298.15, 303.15, and 310.15 K. The fluorescence spectrum was acquired after 1 min from each addition setting the instrument (Varian Cary Eclipse Spectrophotometer) with the following parameters: λEXC = 295 nm; slit 10 nm; acquisition from 310 to 500 nm). The fluorescence at the maximum intensity was employed to obtain the Stern-Volmer plots using the equation:

$$\frac{F_0}{F} = 1 + K_{SV}[Q] = 1 + K_q\tau_0[Q] \tag{4}$$

F_0 and F represent the fluorescence intensities of the enzyme before and after the addition of inhibitor, respectively. [Q] represents the concentration of the compounds studied; Ksv represents the Stern-Volmer quenching constant. If the quenching is dynamic, the Stern-Volmer constant will be represented by K_D; otherwise, this constant will be described as K_{sv}. K_q is the biomolecule quenching rate and it is related with τ_0, the average lifetime of the fluorophore in the absence of quencher protein (approximately 10 − 8 s for α-Glu and α-Amy). The binding constant (K_a) and the number of binding sites n were calculated with the following equation:

$$log\frac{F_0\ \ \text{-}\ F}{F} = logK_a + nlog[Q] \tag{5}$$

4.6. Molecular docking analysis

Due to the absence of the related solved structure of α-Glu in the Protein Data Bank, it would have been necessary to proceed with the construction of a homology model [69]. After 2022, the AphaFold protein structure database (https://alphafold.ebi.ac.uk) provided 3D protein models with high-accuracy counting more than 200 million entries [70,71]. The α-glucosidase model was first prepared and minimized by Protein preparation wizard. The putative binding site was identified through SiteMap software that allowed to generate a ranking of five possible druggable binding pockets based on the site score output and the best-one was then used for the molecular docking calculation. Specifically, starting from site 1, the following coordinates were obtained by Grid generation experiment: 14.61 (x), 2.13 (y), 1.91 (z), 10 x 10 x 10 as innerbox, and 36.76 x 36.76 x 36.76 as outerbox. The composition of the α-Glu binding site includes the following interacting residues: Asp68, Ser156, Phe157, Phe177, Asp214, His239, Asn241, His245, Glu276, Ala278, Phe300, Glu304, Thr307, Ser308, Pro309, Arg312, Gln222, Asp349, Gln350 and Asp408. [72]. The.pdb file of human pancreatic α-amylase (PDB ID: 4 W93) was downloaded from Protein Data Bank. The α-amylase is cocrystallized with montbretin A as specific inhibitor. The grid box was centered in the binding site of protein, with grid centre set to –7.28 (x), 7.43 (y) and –18.44 (z), 10 x 10 x 10 as innerbox, and 30 x 30 x 30 as outerbox. The composition of the α-Amy binding site includes: Trp58, Trp59, Tyr62, Val98, His101, Tyr151, Leu162, Thr163, Leu165, Arg195, Ala198, Lys200, His201, Glu233, Glu240, Ile235, His299 and Asp300 as reported previously [72]. The.sdf file of acarbose was downloaded from PubChem (https://pubchem.ncbi.nlm.nih.gov ID code: 41774). Obovatol (**1**) and its analogues were drawn using ChemDraw and saved in.sdf file. Then, the library was prepared by LigPrep software, generating all the possible tautomers and protonation states (pH = 7.4 ± 1.0) for each compound. The obtained structures were minimized by OPLS3. The molecular docking studies were performed using Glide interfaced with Maestro. In docking calculation, protein was treated as rigid and ligands as flexible. Glide were compiled and run in OSX Yosemite (10.10.5) environment. The analysis of docking outcomes was carried out by Maestro (Version 11), and figures of 3D models were generated by Pymol (2.3.5). For mixed-type inhibitors **22** and **27**, other potential binding sites different from the catalytic one were evaluated, four obtained by sitemap and another recently proposed in the literature [55]. For each binding site, the molecular interaction with both molecules was studied and the calculated ΔG_{bind} energies are reported in the Table S1 (see supporting). The best interaction was collected in the allosteric site composed by the following residue (Table S2, line 1): Thr287, Ala289, Ala290, Tyr292, Glu293, Val294, Ser295, His258. Arg259, Met261, Lys262, Asn263, Val265, Gly268, Arg269, Glu270, Ile271, Met272, Thr273 and Lys12.

4.7. Electronic circular dichroism spectra measurements

ECD spectra were recorded on a Jasco J715 spectropolarimeter equipped with a single position Peltier temperature control set at 37 °C, and a quartz cuvette with a 1 cm path length was used for all ECD experiments. CD measurements were performed in the range 200–260 nm in the presence or absence of the tested compounds with the following parameters: scanning rate 50 nm/min, data pitch 0.2 nm, digital integration time (D.I.T) 4 s, band width 2.0 nm. Each ECD spectrum was an average of at least five scans. For each experiment, the α-glucosidase (0.5 μM in 10 mM phosphate buffer, pH 7.2) was titrated with increasing aliquots of natural lead or analogues, thus the concentration of tested compounds was increased from 0:1 to 6:1 for **1**, **11**, **22**, **26** and **27.** The spectra were collected after each addition and corrected by subtraction of the blank (100 mM phosphate buffer). ECD spectra of **1**, **11**, **22**, **26** and **27**, at the highest concentration tested, were acquired under the same conditions. The changes of secondary structures of α-glucosidase were estimated with the secondary Structure Estimation software included in the JASCO Spectra Manager software. The percentage of secondary structure, including α-helix, β-sheet, β-turn and random coil, was estimated by the Jasco J-715 accessory secondary structure analysis program according to Yang's equation.

4.8. Surface plasmon resonance imaging measurements

We performed SPRI experiments using an SPR imager apparatus (GWC Technologies, U.S.A.) and analyzed the detected images by using V++ software (version 4.0, Digital Optics Limited, New Zealand) and the ImageJ 1.32j software package (National Institutes of Health, U.S.A.). SPRI image data (pixel intensity, 0–255 scale) were converted into percentage of reflectivity (%R) using the equation $\%R = 100 \times 0.85I_p/I_s$ where I_p and I_s refer to the reflected light intensity detected using p- and s-polarized light, respectively. The SPRI curves were obtained by plotting the average pixel values (0–255 grey level scale) referring to the selected regions of interest (ROIs) of the SPR images as a function of time. A microfluidic device with six parallel microchannels (80 μm depth, 1.4 cm length, 400 μm width) was used for the study to allow independent control of interactions occurring on six different regions of the SPRI gold surface. The device was fabricated in poly (dimethylsiloxane) (PDMS) polymer by a replica molding technique. PEEK tubes (UpChurch Scientific) were inserted into the microfluidic device to connect the microfluidic cell to an Ismatec IPC (Ismatec SA, Switzerland) peristaltic pump. A refractive index matching liquid was used to obtain the optical contact between the gold substrate and the prism. Phosphate buffered saline (PBS) (137 mM NaCl, 2.7 mM KCl, 10 mM phosphate buffer, pH 7.4) was obtained from VWR (Italy). Dithiobis(N)succinimidylpropionate (DTSP) and Trizma solution (1 M in water) were purchased from Merck (Italy). We used ultrapure water produced with a Milli-Q Integral S3 system (Millipore, Italy) for all the experiments. SPRI gold substrates (Xantec bioanalytics GmbH, Germany) were washed with ultrapure water (Milli-Q water) and ethanol and dried with a stream of nitrogen gas. The substrates were cleaned with UV/ozone for 5 min, immersed in ethanol for 10 min and dried with a nitrogen stream. The functionalization of the gold surface can be referred to in our previously published paper [73]. Compounds **1**, **11**, **22**, **26** and **27** were tested at 200–800 μM in PBS buffer, (prepared by dilutions from stock solutions in methanol ranging from 170 to 340 mM). the solutions were injected onto the surface of the α-Glu and α-Amy, at a flow rate of 15 μL/min, and at room temperature. Our microfluidic device bearing six parallel microchannels allows us to simultaneously compare the binding of different derivates to both immobilized enzymes. The complex was allowed to associate for 1320 s to reach the steady-state and dissociate for 600 s. The bound ligand compound was then desorbed and the α-Glu and α-Amy coating surface was regenerated using pulses of 2 mM NaOH solution after each measurement.

4.9. Biological evaluation

The HCT-116 colon cancer cell line purchased from American Type Culture Collection (ATCC, Manassas, VA, USA) was cultured at 37° C in Dulbecco's Modified Eagle's Medium (DMEM) (Gibco, Paisley, UK), supplemented with 10 % heat-inactivated fetal bovine serum and 100 U/mL penicillin and 100 μg/mL streptomycin, at 37 °C and 5 % CO_2, as already described [74–76]. For morphological assessment by phase contrast inverted microscope, the cells were seeded on a coverslip in 24-well plates at a density of 5×10^4 cells/well. After 24 h cells were treated for 24 h with compound dilutions of ½ IC_{50}, IC_{50} and 2 × IC_{50} for α-Glu inhibition with respect to untreated control cells. Morphology was observed under a phase contrast inverted microscope (Carl Zeiss, Oberkochen, Germany) at 200X. For fluorescence staining with acridine orange/ethidium bromide (AO/EB), after 24 h of treatment, the coverslips were washed twice with PBS and stained for a few min with 200 μL of the Acridine Orange (100 μg/mL), Ethidium Bromide (100 μg/mL) mixture (1:1, v/v) and then washed three times with PBS. Cells were immediately observed under a fluorescent microscopy (Carl Zeiss, Oberkochen, Germany) at 640 × magnification. The cytotoxic activity of selected compounds, was determined by using MTT assay, as already described [77,78]. Cells were plated to a density of 15×10^3 cells/well in 96-well plates for 24 h. Then, culture medium containing various concentrations of all compounds (20, 40, 80, 160, 320 μM) were added and incubated for 24 h at 37 °C. After that, medium was removed and cells washed three times with phosphate-buffered saline solution. Fresh medium containing (0.5 mg/mL of Thiazolyl Blue Tetrazolium Bromide (Merck, Darmstadt, Germany) in phosphate buffer saline (PBS) was added and incubated for 2 h. Culture liquid was removed and cells were lysed in 100 μl of dimethyl sulfoxide (DMSO). The absorbance of mixture was measured at 570 nm using a 96-well plate reader (Spark® 20 M Tecan Trading AG, Switzerland). The percentage of cell viability compared to untreated control cells was calculated after subtraction of the blank. The IC_{50} (the concentration able to inhibit 50 % of cell growth) was calculated using a dose–response model, obtained from sigmoidal fitting of response curves of percent inhibition versus logarithmic concentration, using Graph Pad Prism software. Each result was the mean value of three different experiments performed in triplicate.

Funding

This research was funded by MUR ITALY PRIN 2022 PNRR (Project No. P2022MWY3P) and PRIN 2022 (Project No. 2022R9WCZS), PNRR-M4C2, project "SiciliAn MicronanOTecH Research And Innovation Center-SAMOTHRACE" ECS_00000022 and by the French Ministère de l'Enseignement Supérieur, de la Recherche et de l'Innovation, the CNRS and the Institut Universitaire de France.

CRediT authorship contribution statement

Claudia Sciacca: Writing – original draft, Methodology, Investigation, Formal analysis. **Nunzio Cardullo:** Writing – review & editing, Validation, Methodology, Investigation, Formal analysis. **Luana Pulvirenti:** Validation, Investigation, Formal analysis. **Gabriele Travagliante:** Validation, Investigation, Formal analysis. **Alessandro D'Urso:** Writing – review & editing, Visualization, Resources, Funding acquisition. **Roberta D'Agata:** Data curation, Formal analysis, Investigation, Methodology, Validation, Writing – original draft. **Emanuela Peri:** Conceptualization, Formal analysis, Methodology, Writing – original draft. **Patrizia Cancemi:** Investigation, Resources, Validation, Visualization, Writing – original draft. **Anaëlle Cornu:** Visualization, Formal analysis. **Denis Deffieux:** Visualization, Validation, Formal analysis. **Laurent Pouységu:** Validation, Supervision, Methodology, Formal analysis. **Stéphane Quideau:** Writing – review & editing, Visualization, Supervision, Resources, Conceptualization. **Vera Muccilli:** Writing – review & editing, Visualization, Supervision, Resources, Project administration, Funding acquisition, Conceptualization.

Declaration of competing interest

The authors declare that they have no known competing financial interests or personal relationships that could have appeared to influence the work reported in this paper.

Acknowledgements

The authors gratefully acknowledge the Bio-Nanotech Research and Innovation Tower of the University of Catania (BRIT; project PONa3_00136 financed by Italian MUR) to allow the utilization of the Synergy H1 microplate reader. This work has also benefited from the

analytical facilities of the CESAMO platform at the University of Bordeaux.

Appendix A. Supplementary data

Supplementary data to this article can be found online at https://doi.org/10.1016/j.bioorg.2024.107392.

References

[1] E.W.C. Chan, S.K. Wong, H.T. Chan, A short review on the chemistry, pharmacological properties and patents of obovatol and obovatol (neolignans) from Magnolia obovata, Nat. Prod. Sci. 17 (3) (2021) 141–150, https://doi.org/10.20307/nps.2021.27.3.141.

[2] J. Patočka, A. Strunecká, Expectations of biologically active compounds of the genus Magnolia in biomedicine, J. Appl. Biomed. 4 (2006) 171–178, https://doi.org/10.32725/jab.2006.019.

[3] J. Ock, H.S. Han, S.H. Hong, S.Y. Lee, Y.M. Han, B.M. Kwon, K. Suk, Obovatol attenuates microglia-mediated neuroinflammation by modulating redox regulation, B. J. Pharmacol. 159 (8) (2010) 1646–1662, https://doi.org/10.1111/j.1476-5381.2010.00659.x.

[4] N. Cardullo, F. Monti, V. Muccilli, R. Amorati, A. Baschieri, Reaction with ROO center dot and HOO center dot radicals of Honokiol-related neolignan antioxidants, Molecules 28 (2) (2023) 735, https://doi.org/10.3390/molecules28020735.

[5] Y. Lim, J.S. Kwon, D.W. Kim, S.H. Lee, R.K. Park, J.J. Lee, J.T. Hong, H.S. Yoo, B. M. Kwon, Y.P. Yun, Obovatol from Magnolia obovata inhibits vascular smooth muscle cell proliferation and intimal hyperplasia by inducing p21(Cip1), Atherosclerosis 210 (2) (2010) 372–380, https://doi.org/10.1016/j.atherosclerosis.2009.11.037.

[6] N. Cardullo, V. Barresi, V. Muccilli, G. Spampinato, M. D'Amico, D.F. Condorelli, C. Tringali, Synthesis of bisphenol neolignans inspired by honokiol as antiproliferative agents, Molecules 25 (3) (2020) 733, https://doi.org/10.3390/molecules25030733.

[7] W.S. Choi, T.H. Lee, S.J. Son, T.G. Kim, B.M. Kwon, H.U. Son, S.U. Kim, S.H. Lee, Inhibitory effect of obovatol from Magnolia obovata on the Salmonella type III secretion system, J. Antibiot. 70 (11) (2017) 1065–1069, https://doi.org/10.1038/ja.2017.98.

[8] F. Amblard, B. Govindarajan, B. Lefkove, K.L. Rapp, M. Detorio, J.L. Arbiser, R. F. Schinazi, Synthesis, cytotoxicity, and antiviral activities of new neolignans related to honokiol and magnolol, Bioorg. Med. Chem. Lett. 17 (16) (2007) 4428–4431, https://doi.org/10.1016/j.bmcl.2007.06.024.

[9] D.K. Choi, S. Koppula, K. Suk, Inhibitors of microglial neurotoxicity: focus on natural products, Molecules 16 (2) (2011) 1021–1043, https://doi.org/10.3390/molecules16021021.

[10] H.C. Ou, F.P. Chou, T.M. Lin, C.H. Yang, W.H.H. Sheu, Protective effects of honokiol against oxidized LDL-induced cytotoxicity and adhesion molecule expression in endothelial cells, Chem. Biol. Interact. 161 (1) (2006) 1–13, https://doi.org/10.1016/j.cbi.2006.02.006.

[11] J.H. Oh, L.L. Kang, J.O. Ban, Y.H. Kim, K.H. Kim, S.B. Han, J.T. Hong, Anti-inflammatory effect of 4-O-methylhonokiol, a novel compound isolated from Magnolia officinalis through inhibition of NF-kappa B, Chem. Biol. Interact. 180 (3) (2009) 506–514, https://doi.org/10.1016/j.cbi.2009.03.014.

[12] J. Park, J. Lee, E.S. Jung, Y. Park, K. Kim, B. Park, K.S. Jung, E. Park, J. Kim, D. Park, In vitro antibacterial and anti-inflammatory effects of honokiol and magnolol against Propionibacterium sp, Eur. J. Pharmacol. 496 (1–3) (2004) 189–195, https://doi.org/10.1016/j.ejphar.2004.05.047.

[13] C.C. Shen, C.L. Ni, Y.C. Shen, Y.L. Huang, C.H. Kuo, T.S. Wu, C.C. Chen, Phenolic constituents from the stem bark of magnolia officinalis, J. Nat. Prod. 72 (1) (2009) 168–171, https://doi.org/10.1021/np800494e.

[14] Q. Xu, L.T. Yi, Y. Pan, X. Wang, Y.C. Li, J.M. Li, C.P. Wang, L.D. Kong, Antidepressant-like effects of the mixture of honokiol and magnolol from the barks of Magnolia officinalis in stressed rodents, Prog. Neuropsychopharmacol. Biol. Psychiatry. 32 (3) (2008) 715–725, https://doi.org/10.1016/j.pnpbp.2007.11.020.

[15] C. Sciacca, N. Cardullo, L. Pulvirenti, A. Di Francesco, V. Muccilli, Evaluation of honokiol, magnolol and of a library of new nitrogenated neolignans as pancreatic lipase inhibitors, Bioorg Chem 134 (2023) 106555, https://doi.org/10.1016/j.bioorg.2023.106455.

[16] N.S. Reddy Basi V., Yadav Jhillu S., Subramanyam R., Synthesis of magnolol and its analogue compounds, 2014. Patent: CN2010800648512A.

[17] C.M. Chen, Y.C. Liu, A concise synthesis of honokiol, Tetrahedron Lett. 50 (10) (2009) 1151–1152, https://doi.org/10.1016/j.tetlet.2008.12.095.

[18] A. Kumar, U.K. Singh, A. Chaudhary, Honokiol analogs: a novel class of anticancer agents targeting cell signaling pathways and other bioactivities, Future Med. Chem. 5 (7) (2013) 809–829, https://doi.org/10.4155/fmc.13.32.

[19] V.P. Kumar, R.G. Reddy, D.D. Vo, S. Chakravarty, S. Chandrasekhar, R. Grée, Synthesis and neurite growth evaluation of new analogues of honokiol, a neolignan with potent neurotrophic activity, Bioorg. Med. Chem. Lett. 22 (3) (2012) 1439–1444, https://doi.org/10.1016/j.bmcl.2011.12.015.

[20] A. Fuchs, R. Baur, C. Schoeder, E. Sigel, C.E. Muller, Structural analogues of the natural products magnolol and honokiol as potent allosteric potentiators of GABA (A) receptors, Bioorg. Med. Chem. 22 (24) (2014) 6908–6917, https://doi.org/10.1016/j.bmc.2014.10.027.

[21] X. Wang, Q.Q. Liu, Y. Fu, R.B. Ding, X. Qi, X. Zhou, Z. Sun, J.L. Bao, Magnolol as a potential anticancer agent: a proposed mechanistic insight, Molecules 27 (19) (2022) 6441, https://doi.org/10.3390/molecules27196441.

[22] J. Chen, C. Tao, X. Huang, Z. Chen, L. Wang, X. Li, M. Ma, Z. Wu, CT2-3, a novel magnolol analogue suppresses NSCLC cells through triggering cell cycle arrest and apoptosis, Bioorg. Med. Chem. 28 (6) (2020) 115352, https://doi.org/10.1016/j.bmc.2020.115352.

[23] K. Stout, M. Bernaskova, G.W. Miller, A. Hufner, W. Schuehly, Bioinspired honokiol analogs and their evaluation for activity on the norepinephrine transporter, Molecules 23 (10) (2018) 2536, https://doi.org/10.3390/molecules23102536.

[24] C. Yang, L.L. Song, Z. Miao, L.Y. Jiang, T. Li, X.Y. Zhi, X.J. Hao, H. Cao, Discovery of novel obovatol-based phenazine analogs as potential antifungal agents: synthesis and biological evaluation in vitro, Z. Naturforschung b. 76 (3–4) (2021) 173–179, https://doi.org/10.1515/znb-2020-0158.

[25] M.S. Lee, J.E. Yang, E.H. Choi, J.K. In, S.Y. Lee, H. Lee, J.T. Hong, H.W. Lee, Y. G. Suh, J.K. Jung, Synthesis of obovatol derivatives and their preliminary evaluation as antitumor agents, Bull. Korean Chem. Soc. 28 (9) (2007) 1601–1604, https://doi.org/10.5012/bkcs.2007.28.9.1601.

[26] L. Pulvirenti, V. Muccilli, N. Cardullo, C. Spatafora, C. Tringali, Chemoenzymatic synthesis and alpha-glucosidase inhibitory activity of dimeric neolignans inspired by magnolol, J. Nat. Prod. 80 (5) (2017) 1648–1657, https://doi.org/10.1021/acs.jnatprod.7b00250.

[27] F.M. Djeujo, E. Ragazzi, M. Urettini, B. Sauro, E. Cichero, M. Tonelli, G. Froldi, Magnolol and luteolin inhibition of alpha-glucosidase activity: kinetics and type of interaction detected by in vitro and in silico studies, Pharmaceuticals 15 (2) (2022) 205, https://doi.org/10.3390/ph15020205.

[28] C.M. Hu, W.J. Wang, Y.N. Ye, Y. Kang, J. Lin, P.P. Wu, D.L. Li, L.P. Bai, X.T. Xu, B. Q. Li, K. Zhang, Novel cinnamic acid magnolol derivatives as potent alpha-glucosidase and alpha-amylase inhibitors: synthesis, in vitro and in silico studies, Bioorg. Chem. 116 (2021) 105291, https://doi.org/10.1016/j.bioorg.2021.105291.

[29] J. Chu, R. Yang, W. Cheng, L. Cui, H. Pan, J. Liu, Y. Guo, Semisynthesis, biological activities, and mechanism studies of Mannich base analogues of magnolol/honokiol as potential α-glucosidase inhibitors, Bioorg. Med. Chem. 75 (2022) 117070, https://doi.org/10.1016/j.bmc.2022.117070.

[30] K. Jones, L. Sim, S. Mohan, J. Kumarasamy, H. Liu, S. Avery, H.Y. Naim, R. Quezada-Calvillo, B.L. Nichols, B.M. Pinto, D.R. Rose, Mapping the intestinal alpha-glucogenic enzyme specificities of starch digesting maltase-glucoamylase and sucrase-isomaltase, Bioorg. Med. Chem. 19 (13) (2011) 3929–3934, https://doi.org/10.1016/j.bmc.2011.05.033.

[31] L. Sim, C. Willemsma, S. Mohan, H.Y. Naim, B.M. Pinto, D.R. Rose, Structural basis for substrate selectivity in human maltase-glucoamylase and sucrase-isomaltase N-terminal domains, J. Biol. Chem. 285 (23) (2010) 17763–17770, https://doi.org/10.1074/jbc.M109.078980.

[32] T. Fujisawa, H. Ikegami, K. Inoue, Y. Kawabata, T. Ogihara, Effect of two α-glucosidase inhibitors, voglibose and acarbose, on postprandial hyperglycemia correlates with subjective abdominal symptoms, Metabolism 54 (3) (2005) 387–390, https://doi.org/10.1016/j.metabol.2004.10.004.

[33] N. Kaur, V. Kumar, S.K. Nayak, P. Wadhwa, P. Kaur, S.K. Sahu, Alpha-amylase as molecular target for treatment of diabetes mellitus: A comprehensive review, Chem. Biol. Drug Des. 98 (4) (2021) 539–560, https://doi.org/10.1111/cbdd.13909.

[34] Y. Dong, L. Sui, F. Yang, X. Ren, Y. Xing, Z. Xiu, Reducing the intestinal side effects of acarbose by baicalein through the regulation of gut microbiota: An in vitro study, Food Chem. 394 (2022) 133561, https://doi.org/10.1016/j.foodchem.2022.133561.

[35] G. Evano, N. Blanchard, M. Toumi, Copper-mediated coupling reactions and their applications in natural products and designed biomolecules synthesis, Chem. Rev. 108 (8) (2008) 3054–3131, https://doi.org/10.1021/cr8002505.

[36] N.H. Nguyen, N.M.A. Tran, T.H. Duong, G.V. Vo, α-Glucosidase inhibitory activities of flavonoid derivatives isolated from Bouea macrophylla: in vitro and in silico studies, RSC Adv. 13 (12) (2023) 8190–8201, https://doi.org/10.1039/d3ra00650f.

[37] M. Nawaz, M. Taha, F. Qureshi, N. Ullah, M. Selvaraj, S. Shahzad, S. Chigurupati, A. Waheed, F.A. Almutairi, Structural elucidation, molecular docking, α-amylase and α-glucosidase inhibition studies of 5-amino-nicotinic acid derivatives, BMC Chem. 14 (1) (2020) 43, https://doi.org/10.1186/s13065-020-00695-1.

[38] S.M. Farid, M. Noori, M.N. Montazer, M.K. Ghomi, M. Mollazadeh, N. Dastyafteh, C. Irajie, K. Zomorodian, S.S. Mirfazli, S. Mojtabavi, M.A. Faramarzi, B. Larijani, A. Iraji, M. Mahdavi, Synthesis and structure-activity relationship studies of benzimidazole-thioquinoline derivatives as α-glucosidase inhibitors, Sci. Rep. 13 (1) (2023), https://doi.org/10.1038/s41598-023-31080-2.

[39] H. Wali, A. Anwar, S. Shamim, K.M. Khan, M. Mahdavi, U. Salar, B. Larijani, S. Perveen, M. Taha, M.A. Faramarzi, Synthesis, in vitro, and in silico studies of newly functionalized quinazolinone analogs for the identification of potent alpha-glucosidase inhibitors, J. Iran. Chem. Soc. 18 (8) (2021) 2017–2034, https://doi.org/10.1007/s13738-021-02159-2.

[40] S. Horikoshi, T. Watanabe, M. Kamata, Y. Suzuki, N. Serpone, Microwave-assisted organic syntheses: microwave effect on intramolecular reactions - the Claisen rearrangement of allylphenyl ether and 1-allyloxy-4-methoxybenzene, RSC Adv. 5 (110) (2015) 90272–90280, https://doi.org/10.1039/C5RA18039B.

[41] E. Buck, Z.J. Song, D. Tschaen, P.G. Dormer, R.P. Volante, P.J. Reider, Ullmann diaryl ether synthesis: Rate acceleration by 2,2,6,6-tetramethylheptane-3,5-dione, Org. Lett. 4 (9) (2002) 1623–1626, https://doi.org/10.1021/ol025839t.

[42] A. Ouali, J.F. Spindler, A. Jutand, M. Taillefer, Nitrogen ligands in copper-catalyzed arylation of phenols: Structure/activity relationships and applications, Adv. Synth. Catal. 349 (11–12) (2007) 1906–1916, https://doi.org/10.1002/adsc.200600628.

[43] A. Ozanne, L. Pouységu, D. Depernet, B. François, S. Quideau, A stabilized formulation of IBX (SIBX) for safe oxidation reactions including a new oxidative demethylation of phenolic methyl aryl ethers, Org. Lett. 5 (16) (2003) 2903–2906, https://doi.org/10.1021/ol0349965.

[44] L. Pouységu, T. Sylla, T. Garnier, L.B. Rojas, J. Charris, D. Deffieux, S. Quideau, Hypervalent iodine-mediated oxygenative phenol dearomatization reactions, Tetrahedron 66 (31) (2010) 5908–5917, https://doi.org/10.1016/j.tet.2010.05.078.

[45] N. Cardullo, V. Muccilli, L. Pulvirenti, A. Cornu, L. Pouységu, D. Deffieux, S. Quideau, C. Tringali, C-glucosidic ellagitannins and galloylated glucoses as potential functional food ingredients with anti-diabetic properties: a study of α-glucosidase and α-amylase inhibition, Food Chem. 313 (2020) 126099, https://doi.org/10.1016/j.foodchem.2019.126099.

[46] N. Cardullo, G. Floresta, A. Rescifina, V. Muccilli, C. Tringali, Synthesis and in vitro evaluation of chlorogenic acid amides as potential hypoglycemic agents and their synergistic effect with acarbose, Bioorg. Chem. 117 (2021) 105458, https://doi.org/10.1016/j.bioorg.2021.105458.

[47] N. Cardullo, G. Catinella, G. Floresta, V. Muccilli, S. Rosselli, A. Rescifina, M. Bruno, C. Tringali, Synthesis of rosmarinic acid amides as antioxidative and hypoglycemic agents, J. Nat. Prod. 82 (3) (2019) 573–582, https://doi.org/10.1021/acs.jnatprod.8b01002.

[48] T. Luthra, R. Agarwal, M. Estari, U. Adepally, S. Sen, A novel library of -arylketones as potential inhibitors of α-glucosidase: their design, synthesis, in vitro and in vivo studies, Sci. Rep. 7 (2017), https://doi.org/10.1038/s41598-017-13798-y.

[49] J. Lin, D. Xiao, L. Lu, B. Liang, Z. Xiong, X. Xu, New β-carboline derivatives as potential α-glucosidase inhibitor: synthesis and biological activity evaluation, J. Mol. Struct. 128 (2023) 135279, https://doi.org/10.1016/j.molstruc.2023.135279.

[50] S.A. Halim, S. Jabeen, A. Khan, A. Al-Harrasi, Rational design of novel inhibitors of α- glucosidase: an application of quantitative structure activity relationship and structure-based virtual screening, Pharmaceuticals 14 (5) (2021) 482, https://doi.org/10.3390/ph14050482.

[51] A. Daina, O. Michielin, V. Zoete, SwissADME: a free web tool to evaluate pharmacokinetics, drug-likeness and medicinal chemistry friendliness of small molecules, Sci. Rep. 7 (2017) 42717, https://doi.org/10.1038/srep42717.

[52] M. Ezati, F. Ghavamipour, H. Adibi, K. Pouraghajan, S.S. Arab, R.H. Sajedi, R. Khodarahmi, Design, synthesis, spectroscopic characterizations, antidiabetic, in silico and kinetic evaluation of novel curcumin-fused aldohexoses, Spectrochim Acta Part A Mol. Biomol. Spectrosc. 285 (2023) 121806, https://doi.org/10.1016/j.saa.2022.121806.

[53] M. Ezati, F. Ghavamipour, N. Khosravi, R.H. Sajedi, M. Chalabi, A. Farokhi, H. Adibi, R. Khodarahmi, Synthesis and potential antidiabetic properties of curcumin-based derivatives: an in vitro and in silico study of α-glucosidase and α-amylase inhibition, Med. Chem. 19 (1) (2023) 99–117, https://doi.org/10.2174/1573406418666220509101854.

[54] M. Ezati, F. Ghavamipour, M.M.H. Yazdi, K. Sadrjavadi, R.H. Sajedi, H. Adibi, R. Khodarahmi, Synthesis, in silico, in vitro and in vivo studies of novel natural-based arylidenes curcumin as potential glycohydrolase digestive enzymes inhibitors, J. Biomol. Struct. Dyn. 41 (22) (2023) 12686–12702, https://doi.org/10.1080/07391102.2023.2175372.

[55] N.U. Rehman, S.A. Halim, M. Al-Azri, M. Khan, A. Khan, K. Rafiq, A. Al-Rawahi, R. Csuk, A. Al-Harrasi, Triterpenic acids as non-competitive α-glucosidase inhibitors from Boswellia elongata with structure-activity relationship, In Vitro and in Silico Studies, Biomolecules 10 (5) (2020) 751, https://doi.org/10.3390/biom10050751.

[56] Y. Zheng, W. Yang, W. Sun, S. Chen, D. Liu, X. Kong, J. Tian, X. Ye, Inhibition of porcine pancreatic α-amylase activity by chlorogenic acid, J. Funct. Foods. 64 (2020) 103587, https://doi.org/10.1016/j.jff.2019.103587.

[57] Z. Allahdad, M. Varidi, R. Zadmard, A.A. Saboury, Spectroscopic and docking studies on the interaction between caseins and β-carotene, Food Chem. 255 (2018) 187–196, https://doi.org/10.1016/j.foodchem.2018.01.143.

[58] A. Wen, Y. Chen, S. Yuan, H. Yu, Y. Guo, Y. Cheng, Y. Xie, H. Qian, W. Yao, Elucidation of the binding behavior between tetracycline and bovine casein by multi-spectroscopic and molecular simulation methods, J. Lumin. 260 (2023) 119879, https://doi.org/10.1016/j.jlumin.2023.119879.

[59] X. Peng, G.W. Zhang, Y.J. Liao, D.M. Gong, Inhibitory kinetics and mechanism of kaempferol on alpha-glucosidase, Food Chem. 190 (2016) 207–215, https://doi.org/10.1016/j.foodchem.2015.05.088.

[60] R. D'Agata, N. Bellassai, G. Spoto, Exploiting the design of surface plasmon resonance interfaces for better diagnostics: a perspective review, Talanta 125033 (2024), https://doi.org/10.1016/j.talanta.2023.125033.

[61] G. Spoto, M. Minunni, Surface plasmon resonance imaging: what next? J. Phys. Chem. Lett. 3 (2012) 2682–2691, https://doi.org/10.1021/jz301053n.

[62] G. Grasso, R. D'Agata, L. Zanoli, G. Spoto, Microfluidic networks for surface plasmon resonance imaging real-time kinetics experiments, Microchem. J. 93 (1) (2009) 82–86, https://doi.org/10.1016/j.microc.2009.05.001.

[63] C.Y. Lim, N.A. Owens, R.D. Wampler, Y. Ying, J.H. Granger, M.D. Porter, M. Takahashi, K. Shimazu, Succinimidyl ester surface chemistry: implications of the competition between aminolysis and hydrolysis on covalent protein immobilization, Langmuir 30 (43) (2014) 12868–12878, https://doi.org/10.1021/la503439g.

[64] R.L. Rich, G.A. Papalia, P.J. Flynn, J. Furneisen, J. Quinn, J.S. Klein, P.S. Katsamba, M.B. Waddell, M. Scott, J. Thompson, J. Berlier, S. Corry, M. Baltzinger, G. Zeder-Lutzi, A. Schoenemann, A. Clabbers, S. Wieckowski, M.M. Murphy, P. Page, T. E. Ryan, J. Duffner, T. Ganguly, J. Corbin, S. Gautam, G. Anderluh, A. Bavdek, D. Reichmann, S.P. Yadav, E. Hommema, E. Pol, A. Drake, S. Klakamp, T. Chapman, D. Kernaghan, K. Miller, J. Schuman, K. Lindquist, K. Herlihy, M. B. Murphy, R. Bohnsack, B. Andrien, P. Brandani, D. Terwey, R. Millican, R. J. Darling, L. Wang, Q. Carter, J. Dotzlaf, J. Lopez-Sagaseta, I. Campbell, P. Torreri, S. Hoos, P. England, Y. Liu, Y. Abdiche, D. Malashock, A. Pinkerton, M. Wong, E. Lafer, C. Hinck, K. Thompson, C. Di Primo, A. Joyce, J. Brooks, F. Torta, A.B. B. Hagel, J. Krarup, J. Pass, M. Ferreira, S. Shikov, M. Mikolajczyk, Y. Abe, G. Barbato, A.M. Giannetti, G. Krishnamoorthy, B. Beusink, D. Satpaev, T. Tsang, E. Fang, J. Partridge, S. Brohawn, J. Horn, O. Pritsch, G. Obal, S. Nilapwar, B. Busby, G. Gutierrez-Sanchez, R. Das Gupta, S. Canepa, K. Witte, Z. Nikolovska-Coleska, Y.H. Cho, R. D'Agata, K. Schlick, R. Calvert, E.M. Munoz, M.J. Hernaiz, T. Bravman, M. Dines, M.H. Yang, A. Puskas, E. Boni, J.J. Li, M. Wear, A. Grinberg, J. Baardsnes, O. Dolezal, M. Gainey, H. Anderson, J.L. Peng, M. Lewis, P. Spies, Q. Trinh, S. Bibikov, J. Raymond, M. Yousef, V. Chandrasekaran, Y.G. Feng, A. Emerick, S. Mundodo, R. Guimaraes, K. McGirr, Y.J. Li, H. Hughes, H. Mantz, R. Skrabana, M. Witmer, J. Ballard, L. Martin, P. Skladal, G. Korza, I. Laird-Offringa, C.S. Lee, A. Khadir, F. Podlaski, P. Neuner, J. Rothacker, A. Rafique, N. Dankbar, P. Kainz, E. Gedig, M. Vuyisich, C. Boozer, N. Ly, M. Toews, A. Uren, O. Kalyuzhniy, K. Lewis, E. Chomey, B.J. Pak, D.G. Myszka, A global benchmark study using affinity-based biosensors, Anal. Biochem. 386 (2) (2009) 194–216, https://doi.org/10.1016/j.ab.2008.11.021.

[65] M. Conrad, P. Fechner, G. Proll, G. Gauglitz, Comparison of methods for quantitative biomolecular interaction analysis, Anal. Bioanal. Chem. 414 (1) (2022) 661–673, https://doi.org/10.1007/s00216-021-03623-x.

[66] X. Liu, F. Luo, P. Li, Y. She, W. Gao, Investigation of the interaction for three Citrus flavonoids and α-amylase by surface plasmon resonance, Food Res. Int. 97 (2017) 1–6, https://doi.org/10.1016/j.foodres.2017.03.023.

[67] J.H. Kwak, J.K. In, M.S. Lee, E.H. Choi, H. Lee, J.T. Hong, Y.P. Yun, S.J. Lee, S. Y. Seo, Y.G. Suh, J.K. Jung, Concise synthesis of Obovatol: Chemoselective ortho-bromination of phenol and survey of Cu-catalyzed diaryl ether couplings, Arch. Pharm. Res. 31 (12) (2008) 1559–1563, https://doi.org/10.1007/s12272-001-2151-9.

[68] S.P. Henry, T.J. Fernandez, J.P. Anand, N.W. Griggs, J.R. Traynor, H.I. Mosberg, Structural Simplification of a tetrahydroquinoline-core peptidomimetic mu-opioid receptor (MOR) agonist/delta-opioid receptor (DOR) antagonist produces improved metabolic stability, J. Med. Chem. 62 (8) (2019) 4142–4157, https://doi.org/10.1021/acs.jmedchem.9b00219.

[69] M.P. Jacobson, D.L. Pincus, C.S. Rapp, T.J.F. Day, B. Honig, D.E. Shaw, R. A. Friesner, A hierarchical approach to all-atom protein loop prediction, Proteins 55 (2) (2004) 351–367, https://doi.org/10.1002/prot.10613.

[70] J. Jumper, R. Evans, A. Pritzel, T. Green, M. Figurnov, O. Ronneberger, K. Tunyasuvunakool, R. Bates, A. Zidek, A. Potapenko, A. Bridgland, C. Meyer, S.A. A. Kohl, A.J. Ballard, A. Cowie, B. Romera-Paredes, S. Nikolov, R. Jain, J. Adler, T. Back, S. Petersen, D. Reiman, E. Clancy, M. Zielinski, M. Steinegger, M. Pacholska, T. Berghammer, S. Bodenstein, D. Silver, O. Vinyals, A.W. Senior, K. Kavukcuoglu, P. Kohli, D. Hassabis, Highly accurate protein structure prediction with AlphaFold, Nature 596 (7873) (2021) 583–589, https://doi.org/10.1038/s41586-021-03819-2.

[71] M. Varadi, S. Anyango, M. Deshpande, S. Nair, C. Natassia, G. Yordanova, D. Yuan, O. Stroe, G. Wood, A. Laydon, A. Zidek, T. Green, K. Tunyasuvunakool, S. Petersen, J. Jumper, E. Clancy, R. Green, A. Vora, M. Lutfi, M. Figurnov, A. Cowie, N. Hobbs, P. Kohli, G. Kleywegt, E. Birney, D. Hassabis, S. Velankar, AlphaFold Protein Structure Database: massively expanding the structural coverage of protein-sequence space with high-accuracy models, Nucleic Acids Res. 50 (D1) (2022) D439–D444, https://doi.org/10.1093/nar/gkab1061.

[72] A. Kryshchyshyn-Dylevych, L. Radko, N. Finiuk, M. Garazd, N. Kashchak, A. Posyniak, K. Niemczuk, R. Stoika, R. Lesyk, Synthesis of novel indole-thiazolidinone hybrid structures as promising scaffold with anticancer potential, Bioorg. Med. Chem. 50 (2021) 116453, https://doi.org/10.1016/j.bmc.2021.116453.

[73] R. D'Agata, N. Bellassai, M. Allegretti, A. Rozzi, S. Korom, A. Manicardi, E. Melucci, E. Pescarmona, R. Corradini, P. Giacomini, G. Spoto, Direct plasmonic detection of circulating RAS mutated DNA in colorectal cancer patients, Biosens. Bioelectron. 170 (2020) 1112648, https://doi.org/10.1016/j.bios.2020.112648.

[74] M. Barreca, M. Buttacavoli, G. Di Cara, C. D'Amico, E. Peri, V. Spanò, G. Li Petri, P. Barraja, M.V. Raimondi, P. Cancemi, A. Montalbano, Exploring the anticancer activity and the mechanism of action of pyrrolomycins F obtained by microwave-assisted total synthesis, Eur. J. Med. Chem. 253 (2023) 115339, https://doi.org/10.1016/j.ejmech.2023.115339.

[75] M. Massaro, G. Barone, V. Barra, P. Cancemi, A. Di Leonardo, G. Grossi, F. Lo Celso, S. Schenone, C.V. Iborra, S. Riela, Pyrazole [3,4-d] pyrimidine derivatives loaded into halloysite as potential CDK inhibitors, Int. J. Pharm. 599 (2021) 120281, https://doi.org/10.1016/j.ijpharm.2021.120281.

[76] G. Schiera, C.M. Di Liegro, V. Puleo, O. Colletta, A. Fricano, P. Cancemi, G. Di Cara, I. Di Liegro, Extracellular vesicles shed by melanoma cells contain a modified form

of H1.0 linker histone and H1.0 mRNA-binding proteins, Int. J. Oncol. 49 (5) (2016) 1807–1814, https://doi.org/10.3892/ijo.2016.3692.

[77] C. Rizzo, P. Cancemi, M. Buttacavoli, G. Di Cara, C. D'Amico, F. Billeci, S. Marullo, F. D'Anna, Insights about the ability of folate based supramolecular gels to act as targeted therapeutic agents, J. Mater. Chem. B 11 (32) (2023) 7721–7738, https://doi.org/10.1039/D3TB01389H.

[78] G. Raia, S. Marullo, G. Lazzara, G. Cavallaro, S. Marino, P. Cancemi, F. D'Anna, Upcycling of poly(lactic acid) waste: a valuable strategy to obtain ionic liquids, ACS Sustainable Chem. Eng. 11 (50) (2023) 17870–17880, https://doi.org/10.1021/acssuschemeng.3c07024.